arXiv:1602.08153v2 [physics.flu-dyn] 18 Mar 2016

Melting of a nonequilibrium vortex crystal in a fluid film with polymers : elastic versus fluid turbulence

Anupam Gupta[1] **and Rahul Pandit**[2,*]

[1]Department of Physics, University of "Tor Vergata", Via della Ricerca Scientifica 1, 00133 Rome, Italy
[2]Centre for Condensed Matter Theory, Department of Physics, Indian Institute of Science, Bangalore 560012, India
[*]rahul@physics.iisc.ernet.in

ABSTRACT

We perform a direct numerical simulation (DNS) of the forced, incompressible two-dimensional Navier-Stokes equation coupled with the FENE-P equations for the polymer-conformation tensor. The forcing is such that, without polymers and at low Reynolds numbers Re, the film attains a steady state that is a square lattice of vortices and anti-vortices. We find that, as we increase the Weissenberg number $\mathscr{W}i$, a sqeuence of nonequilibrium phase transitions transforms this lattice, first to spatially distorted, but temporally steady, crystals and then to a sequence of crystals that oscillate in time, periodically, at low $\mathscr{W}i$, and quasiperiodically, for slightly larger $\mathscr{W}i$. Finally, the system becomes disordered and displays spatiotemporal chaos and elastic turbulence. We then obtain the nonequilibrium phase diagram for this system, in the $\mathscr{W}i - Re$ plane, and show that (a) the boundary between the crystalline and turbulent phases has a complicated, fractal-type character and (b) the Okubo-Weiss parameter Λ provides us with a natural measure for characterizing the phases and transitions in this diagram.

Introduction

The equilibrium melting transition, from a spatially periodic crystal to a homogeneous liquid, has been studied extensively.[1–6] Nonequilibrium analogues of this transition have been explored in, e.g., the melting of colloidal crystals by shear[7] and the turbulence-induced melting of a periodic array of vortices and anti-vortices in a forced, two-dimensional (2D), fluid film.[6] We elucidate, via extensive direct numerical simulations (DNSs), the nonequilibrium melting of a periodic array of vortices and anti-vortices in a forced, 2D, fluid film with polymer additives; we refer to this periodic array as a nonequilibrium, 2D crystal; this is also called a cellular flow[8,9] in some studies.

We show that such a crystal can be melted either (a) by increasing the Grashof number $\mathscr{G}r$ (or Reynolds numbers Re) number or (b) by increasing the Weissenberg number $\mathscr{W}i$. Case (a) can be thought of as a nonequilibrium melting transition, which is driven by fluid turbulence[6,10,11] and in which the disordered phase is a turbulent fluid that shows dissipation reduction, because of the polymer additives.[12–14] Case (b) is also a nonequilibrium melting transition; in this case the vortex crystal melts into a disordered state, which is a polymeric fluid that shows elastic turbulence[15,16] or rheochaos.[17,18] We show that this system of driven vortices and anti-vortices provides an excellent laboratory for studying the crossover from the dissipation-reduction to the elastic-turbulence regimes in a fluid film.

Case (a), namely, turbulence-induced melting, has been explored in experiments,[10,11] which use a spatially periodic force to impose a nonequilibrium vortex crystal on a fluid film at low Re; this crystal melts, at high Re, into a disodered, nonequilibrium, liquid-type phase. This melting problem has been studied by using linear-stability analysis,[8,9] for the first instability of the vortex crystal, and direct numerical simulations (DNS).[6,19,20] These DNSs have explored the nonequilibrium phase diagram of this driven, dissipative system by using techniques from nonlinear dynamics[6,19,20] and generalizations of order parameters that are used to characterize equilibrium crystals.[1–3,6]

To the best of our knowledge, case (b), namely, elastic-turbulence-induced melting of a vortex crystal, has not been explored in experiments, even though there have been several experimental studies of elastic turbulence[15,16] and the related phenomenon of rheochaos.[17,18] Direct numerical simulations of 2D fluid films with polymer additives have begun to explore the[21,22] elastic-turbulence-induced melting of spatially periodic flows; the Kolmogorov-flow pattern investigated in Ref.[21,22] is a one-dimensional crystal.

The nonequilibrium vortex crystal, whose melting we study, is a 2D crystal. To describe the ordering in this crystal and its subsequent melting, either by elastic or fluid turbulence, we follow the treatment of Ref.,[6] which has investigated this problem in the absence of polymers. In particular, we solve the incompressible, 2D, Navier-Stokes (NS) equation, for the fluid film, coupled to the FENE-P equation, for the polymer-conformation tensor $\mathscr{C}$; this provides a good description of our system if the

Mach number is small and finite-film-thickness and Marangoni-effect corrections can be neglected.[6,23–25] The force we use yields, at low *Re*, a spatially periodic array of vortices and antivortices that is stationary in time; we call this a vortex crystal.

We investigate the stability of this crystal as we increase either (a) the forcing amplitude and, thereby, $\mathscr{G}r$ or *Re* or (b) the polymer-relaxation time τ_p and, hence, $\mathscr{W}i$. We show that time-series of the energy of the fluid, their power spectra, and Poincaré-type maps (see below) can be used to understand the spatiotemporal evolution of this system and its sequence of nonequilibrium transitions (cf., Refs.[6,19,20] for turbulence-induced melting in a fluid film without polymers).

We explore these transitions by using ideas from the density-functional theory of the crystallization of a liquid[1,3–6] to develop order parameters for our vortex crystal. The crystal density is *periodic* in space; the density-functional theory uses its Fourier coefficients as *order parameters*; in particular, the density $\rho(\mathbf{r})$ has the Fourier representation

$$\rho(\mathbf{r}) = \sum_{\mathbf{G}} \rho_{\mathbf{G}} \exp(\imath \mathbf{G}\cdot\mathbf{r}), \tag{1}$$

where $\mathbf{G}$ are the *reciprocal-lattice* vectors; $\rho_{\mathbf{G}}$ are the order parameters of the liquid-to-crystal transition because they have zero mean values in the liquid phase for all nonzero $\mathbf{G}$; the mean density is $\rho_{\mathbf{G}=0}$; liquids are almost incompressible, so, at the liquid-to-crystal transition, the jump in this density is very small. Spatial correlations of the density follow from $g(\mathbf{r}) = \langle\overline{[\rho(\mathbf{x}+\mathbf{r})\rho(\mathbf{x})]}\rangle$, where the angular brackets denote thermal averages; the overline is an average over $\mathbf{x}$. The static structure factor $S(\mathbf{k})$ follows[1,3] from the Fourier transform of $g(\mathbf{r})$. In the isotropic liquid phase g and S depend, respectively, on $r = \mid \mathbf{r} \mid$ and $k = \mid \mathbf{k} \mid$.

It has been noted in Ref.[6] that the Okubo-Weiss field $\Lambda \equiv \det(A)$ can be used in the vortex-crystal instead of $\rho(\mathbf{r})$ in the density-functional theory mentioned above; A has elements $A_{ij} \equiv \partial_i u_j$, with u_j the j^{th} component of the velocity. For an inviscid, incompressible, 2D, fluid the local flow topology can be characterized via the Okubo-Weiss criterion,[26,27] which provides a useful measure of flow properties even if viscosity and wall friction are present.[25,28,29] This criterion states that $\Lambda > 0$, where the flow is vortical, and $\Lambda < 0$, where it is extensional or strain-dominated.[26,27] In a nonequilibrium vortex crystal, $\Lambda(\mathbf{r})$ is a periodic function of $\mathbf{r}$; so it has the Fourier expansion

$$\Lambda(\mathbf{r}) = \sum_{\mathbf{k}} \hat{\Lambda}_{\mathbf{k}} \exp(\imath \mathbf{k}\cdot\mathbf{r}), \tag{2}$$

where $\mathbf{k}$ are the reciprocal-lattice vectors; The coefficients $\hat{\Lambda}_{\mathbf{k}}$ are the natural order parameters for the vortex crystal. In our 2D vortex crystal, the analogue of the static structure factor $S(\mathbf{k})$, for a conventional crystal, is the 2D spectrum

$$E_{\Lambda}(\mathbf{k}) \equiv \langle \hat{\Lambda}_{\mathbf{k}} \hat{\Lambda}_{-\mathbf{k}} \rangle, \tag{3}$$

where the angular brackets denote an average over the nonequilibrium state of our system (and not a Gibbsian thermal average); this state can be independent of time, or it can exhibit periodic or quasiperiodic oscillations, or it can be spatiotemporally chaotic and turbulent, but statistically steady. We define

$$G(\mathbf{r}) = \langle\overline{\Lambda(\mathbf{x}+\mathbf{r})\Lambda(\mathbf{x})}\rangle, \tag{4}$$

an autocorrelation function where spatial Fourier transform is related to $E_{\Lambda}(\mathbf{k})$. This characterizes the spatial correlations in our system. As we show below, the turbulent phase is nearly isotropic so G depends only on $r \equiv \mid \mathbf{r} \mid$ here (this is a very good approximation); and it characterizes the short-range vortical order in our 2D fluid film, exactly as $g(r)$ does in an isotropic liquid at equilibrium. We also follow the spatiotemporal evolution of the polymer-conformation tensor $\mathscr{C}$ and relate it to the spatiotemporal evolution of Λ.

We use the order parameters, defined above, to obtain many interesting results for the elastic-turbulence-induced melting of such a 2D vortex crystal in a fluid film with polymer additives. We first describe our principal results qualitatively. We find that, as we increase *Re* or $\mathscr{W}i$, a rich sequence of transitions leads from the steady, ordered, vortex crystal to the disordered, turbulent state. In Table 1 (column four) we list the types of nonequilibrium phases we encounter: SX is the original, *temporally steady*, crystal, with a square unit cell that is imposed by the force; this is followed by phases of type SXA, which are *temporally steady* crystals that are distorted relative to SX; we then find distorted crystals that displays periodic (OPXA) or quasiperiodic (OQPXA) oscillations in time; finally, the system exhibits *spatiotemporal chaos and turbulence* (SCT). We conjecture that OPXA and OQPXA are actually several (perhaps an infinity) different nonequilibrium spatiotemporal crystals, which are periodic in space and time; given the spatial and temporal resolutions of our calculation, we can identify only some of these. In addition to the order parameters and correlation functions mentioned above, we also examine the spatiotemporal evolution of the polymer-conformation tensor $\mathscr{C}$ in these phases. Our work leads to a rich, nonequilibrium phase diagram for our system. This has not been studied hitherto.

The paper is organized as follows. Section 2 is devoted to the equations which we use to model 2D fluid films with polymer additives and the numerical methods we use. In Sec 3 we present a detailed description of our results. Section 4 is dedicated to a discussion of our results and to conclusions.

Model and Numerical Methods

To study a 2D fluid film with polymer additives, we write the 2D, incompressible, NS and FENE-P equations in terms of the stream-function ψ and the vorticity $\omega = \nabla \times \mathbf{u}(\mathbf{x},\mathbf{t})$, where $\mathbf{u} \equiv (-\partial_y\psi, \partial_x\psi)$ is the fluid velocity at the point $\mathbf{x}$ and time t, as follows (we use the nondimensional form suggested in Ref.[30] for 2D fluid films without polymer additives):

$$D_t\omega = \nabla^2\omega/\Omega + \frac{\mu}{\tau_P}\nabla\times\nabla.[f(r_P)\mathscr{C}] - \alpha\omega + F_\omega; \tag{5}$$

$$\nabla^2\psi = \omega; \tag{6}$$

$$D_t\mathscr{C} = \mathscr{C}.(\nabla\mathbf{u}) + (\nabla\mathbf{u})^T.\mathscr{C} - \frac{f(r_P)\mathscr{C}-\mathscr{I}}{\tau_P}; \tag{7}$$

here, $D_t \equiv \partial_t + \mathbf{u}\cdot\nabla$, the uniform solvent density $\rho = 1$, α is the non-dimensionalized, air-drag-induced friction coefficient, ν is the kinematic viscosity, μ the viscosity parameter for the solute (FENE-P), τ_P the polymer relaxation time, and $F_\omega \equiv -n^3[\cos(nx)+\cos(ny)]/\Omega$ is the non-dimensionalized, spatially periodic force, whose injection wave vector is related to n, $\alpha = n\nu\alpha' k/F_{amp}$, and $\Omega = nF_{amp}/(\nu^2k^3)$, where F_{amp} is the forcing amplitude, and α' is the coefficient of friction. We non-dimensionalize lengths by a factor k/n, with k a wave number or inverse length.[30] The x and y components of the velocity are $u_1 \equiv u$ and $u_2 \equiv v$, respectively. The superscript T denotes a transpose, $\mathscr{C}_{\alpha\beta} \equiv \langle R_\alpha R_\beta\rangle$ are the elements of the polymer-conformation tensor (angular brackets indicate an average over polymer configurations), the identity tensor $\mathscr{I}$ has the elements $\delta_{\alpha\beta}$, $f(r_P) \equiv (L^2-2)/(L^2-r_P^2)$ is the FENE-P potential that ensures finite extensibility, and $r_P \equiv \sqrt{\mathrm{Tr}(\mathscr{C})}$ and L are, respectively, the length and the maximal possible extension of the polymers; and $c \equiv \mu/(\nu+\mu)$ is a dimensionless measure of the polymer concentration[31] (in 3D $c = 0.1$ corresponds, roughly, to 100 ppm for polyethylene oxide[32]).

Our direct numerical simulation (DNS) of Eqs. (5)-(7) uses the MPI code that we have developed to study fluid turbulence with polymer additives in fluid films.[14] We use periodic boundary conditions, a square simulation domain of side $\mathbb{L} = 2\pi$, and N^2 collocation points; these boundary conditions are well suited for studying vortex crystals with square unit cells. We use a fourth-order Runge-Kutta scheme, with time step δt, for time marching and an explicit, fourth-order, central-finite-difference scheme in space and the Kurganov-Tadmor (KT) shock-capturing scheme[33] for the advection term in Eq. (7), because this scheme (see Eq. (7) of Ref.[12]) successfully resolves steep gradients in $\mathscr{C}_{\alpha\beta}$ and, thereby, minimizes dispersion errors. We solve the Poisson equation (6) in Fourier space by using a pseudospectral method and the FFTW library.[34] We choose δt to be small enough to prevent r_P from becoming larger than L (if $r_P > L$, there is a numerical instability). To preserve the symmetric-positive-definite (SPD) nature of $\mathscr{C}$ at all times we adapt to 2D the Cholesky-decomposition scheme of Refs.[12–14,31] In particular, we define $\mathscr{J} \equiv f(r_P)\mathscr{C}$, so Eq. (7) becomes

$$D_t\mathscr{J} = \mathscr{J}.(\nabla\mathbf{u}) + (\nabla\mathbf{u})^T.\mathscr{J} - s(\mathscr{J}-\mathscr{I}) + q\mathscr{J}, \tag{8}$$

where $s = (L^2-2+j^2)/(\tau_P L^2)$, $q = [d/(L^2-2) - (L^2-2+j^2)(j^2-2)/(\tau_P L^2(L^2-2))]$, $j^2 \equiv Tr(\mathscr{J})$, and $d = Tr[\mathscr{J}.(\nabla\mathbf{u}) + (\nabla\mathbf{u})^T.\mathscr{J}]$. Note that $\mathscr{C}$, and hence $\mathscr{J}$, are SPD matrices, so $\mathscr{J} = \mathscr{L}\mathscr{L}^T$, where $\mathscr{L}$ is a lower-triangular matrix with elements ℓ_{ij}, such that $\ell_{ij} = 0$ for $j > i$. We can now use Eq.(8) to obtain, for $1 \le i \le 2$ and $\Gamma_{ij} = \partial_i u_j$,

$$\begin{aligned}
D_t\ell_{11} &= \Gamma_{11}\ell_{11} + \Gamma_{21}\ell_{21} + \frac{1}{2}\left[(q-s)\ell_{11} + \frac{s}{\ell_{11}}\right],\\
D_t\ell_{21} &= \Gamma_{12}\ell_{11} + \Gamma_{21}\frac{\ell_{22}^2}{\ell_{11}} + \Gamma_{22}\ell_{21}\\
&\quad + \frac{1}{2}\left[(q-s)\ell_{21} - s\frac{\ell_{21}}{\ell_{11}^2}\right],\\
D_t\ell_{22} &= -\Gamma_{21}\frac{\ell_{21}\ell_{22}}{\ell_{11}} + \Gamma_{22}\ell_{22}\\
&\quad + \frac{1}{2}\left[(q-s)\ell_{22} - \frac{s}{\ell_{22}}\left(1+\frac{\ell_{21}^2}{\ell_{11}^2}\right)\right].
\end{aligned} \tag{9}$$

Equation(9) preserves the SPD property of $\mathscr{C}$ if $\ell_{ii} > 0$; we enforce this, as in Refs.,[12–14] by considering the evolution of $\ln(\ell_{ii})$ instead of ℓ_{ii}.

In most of our studies, we use a time step $\delta t = 10^{-3}$ to 10^{-4} for $N = 128$; its precise value depends on the value of the polymer relaxation time τ_P; for $\tau_P \simeq 1$, $\delta t = 10^{-3}$ and $\delta t = 10^{-4}$ otherwise ($\tau_P > 1$). Our results do not change significantly if we use $N = 256$ or $N = 1024$ (we have checked this in representative cases). We obtain long time series for several variables (see below) to make sure that the temporal evolution of our system is captured accurately; most of our runs are at least as long as $5\times10^6\delta t$. We monitor the time-evolution of the total kinetic energy $E(t) \equiv \overline{\mathbf{u}^2}$ and calculate the stream

function ψ, vorticity ω, polymer-conformation tensor $\mathscr{C}$, the Okubo-Weiss parameter Λ, and the kinetic energy spectrum $E(k) \equiv \sum_{k-1/2<k'\leq k+1/2} k'^2 \langle |\hat{\psi}(\mathbf{k}',t)|^2 \rangle_t$, where $\langle\rangle_t$ indicates a time average over the statistically steady state. From these we obtain $E_\Lambda(\mathbf{k})$ and $G(\mathbf{r})$, by averaging over 40 configurations of $\Lambda(\mathbf{r})$, which are separated from each other by $10^5\delta t$; to eliminate the effects of initial transients, we remove data from the first 10^6 time steps before we collect data for these averages. From ψ we obtain the velocity and thence the $\mathbf{k} = (1,0)$ component of the Fourier transform $\hat{v}$ of the y component v of $\mathbf{u}$. We use the time series of $E(t)$ to obtain its temporal Fourier transform $E(f)$ and from that the power spectrum $|\, E(f)\,|$, which we use to differentiate between periodic, quasiperiodic, and chaotic temporal evolutions. We also use Poincaré-type sections, namely, plots of $\Im\hat{v}_{(1,0)}$ versus $\Re\hat{v}_{(1,0)}$ at successive times (for the Kolmogorov flow see Ref.[30]).

The equation of motion for a small rigid particle (henceforth, an inertial particle) in an incompressible flow [35,36] assumes the following simple form ,[37,38] if the particle is much heavier than the advecting fluid:

$$\frac{d\boldsymbol{x}}{dt} = \boldsymbol{v}(t); \frac{d\boldsymbol{v}}{dt} = -\frac{\boldsymbol{v}(t) - \boldsymbol{u}[\boldsymbol{x}(t),t]}{\tau_s}; \tag{10}$$

here, $\boldsymbol{v}$ and $\boldsymbol{x}$ are, respectively, the velocity and position of an inertial particle, $\tau_s = (2a^2)/(9\nu\rho_f)$ is the Stokes or response time of the particle, whose ratio with the Kolmogorov dissipation time T_η is the Stokes number $\mathrm{St} = \tau_s/T_\eta$. We assume that the radius of a particle $a \ll \eta$, where η is the dissipation scale of the carrier fluid, and that the particle density is so low that we can neglect interactions between particles. We also assume, as in Ref.,[39] that the polymer additives affect the inertial-particle velocity $\boldsymbol{v}(t)$ only by virtue of their effect on the Eulerian velocity $\boldsymbol{u}[\boldsymbol{x}(t),t]$ of the fluid at the position of the inertial particle. We show below that the spatial distribution of such inertial particles in the flow can also be used to distinguish the nonequilibrium crystalline and turbulent states in our system.

Results

We now present the results of our DNS. We begin with an overview, in the first subsection. In the next subsection, we present the nonequlibrium phase diagram that we obtain from our calculations. We then present the results of our numerical simulations for $n = 4$ and the ranges of parameters given in Table 1. In the third and fourth subsections, respectively, we present our results for $\Omega = 1$ and $\Omega = 22$. In the fifth subsection, we report our results for the order parameters, spatial correlation functions and kinetic energy spectra that we have defined above; and the last subsection contains the results for the spatial patterns of polymers and inertial particles.

Overview

We demonstrate below how our crystal of vortices melts, as we increase τ_P for a fixed, low value of Ω, through a sequence of transitions. At somewhat higher values of Ω, at which the vortex crystal has already reached a melted state because of fluid turbulence, we find that this turbulent state moves first to a frozen state, as we increase τ_P; this frozen state melts again as τ_p increases some more. The air-drag-induced friction delays these transitions; we have checked this in some representative cases. However, to make contact with earlier studies of turbulence-induced melting of a vortex crystal[6,19,20] without polymers, we do not include air-drag-induced friction here. Our conclusions are not altered by this in a qualitative sense.

The steady-state solution,[6,30] of Eq. (5) is $\omega_{s,n} = -n[\cos(nx) + \cos(ny)]$, if $\tau_P = 0$ and $\Omega < \Omega_{s,n}$; here the subscript s stands for steady state. We examine the destabilisation of this solution, by increasing τ_P while we hold Ω fixed, for one representative value of n, namely, $n = 4$ for which $\Omega_{s,4} \simeq 5.657$ (see Ref.[6]). The initial vorticity is taken to be $\omega = \omega_{s,n} + 10^{-4}\sum_{m_1=0,m_2=0}^{2,2}[\sin(m_1x + m_2y) + \cos(m_1x + m_2y)]m_2^2/\sqrt{(m_1^2 + m_2^2)}$; and the system then evolves under the force F_ω. For a fixed value of Ω, we increas τ_P in steps of 0.1; and we carry out simulations for $\Omega = 1,2$ and from then to $\Omega = 26$ in steps of 2. To track the nonequilibrium transitions in our system, say from SXA to SCT, we have also carried out runs in which we increase τ_P in steps of $\simeq 0.01$. We have validated our numerical scheme by comparison with Refs.[6,30] Reference [30] studies a Kolmogorov flow $F_\omega = n\cos(ny)$; and Ref.[6] uses an external force of the form $F_\omega \equiv -n^3[\cos(nx) + \cos(ny)]/\Omega$, which is exactly the same as the one we employ.

For $\tau_P = 0$, and $\Omega < \Omega_{s,n}$, the Λ field shows alternating vortical and extensional regions, which are also referred to as centres and saddles; these are arranged in a two-dimensional square lattice, which we illustrate via pseudocolour plots of Λ, for $n = 4$, in Fig. 1 (a). For $\Omega = 20$, which is well beyond $\Omega_{s,4} \simeq 5.657$, the fluid becomes turbulent; but, on the addition of polymers, τ_P increases, and the fluid again forms a 2D vortex lattice, which we illustrate via pseudocolour plots of Λ, for $n = 4$, in Fig. 1 (b). In Figs. 2 (a) and (b) we show the corresponding pseudocolour plots of stream-funtion ψ, respectively.

Nonequilibrium Phase Diagram

We have carried out a very large number ($\simeq 400$) of DNS studies of our system for a wide range of parameter values in the (τ_P-Ω) plane; only a very small fraction of these parameter values are listed in Table 1. For each one of these parameter

Run	Ω	τ_P	Order
R1 − 1	1	$\tau_P \leq 1.9$	SX
R1 − 2	1	$2 \leq \tau_P \leq 9$	OPXA
R1 − 3	1	$\tau_P \geq 10$	SCT
R22 − 1	22	$\tau_P = 0$	SCT
R22 − 2	22	$0 < \tau_P < 0.45$	OPXA
R22 − 3	22	$\tau_P = 0.5$	SXA
R22 − 4	22	$0.55 < \tau_P < 0.8$	OPXA
R22 − 5	22	$\tau_P \geq 1$	SCT

Table 1. Table indicating the number of the Run (e.g., R1-1), the value of Ω, and the type of order. SX : original, *steady* square crystal (the pattern depends on *n*); SXA : *temporally steady* crystals slightly distorted compared to SX; OPXA : crystal that is distorted slightly relative to SX and temporal oscillations; OQPXA : OPXA but with *quasiperiodic temporal oscillations*; SCT : disordered phase with *spatiotemporal chaos and turbulence*. We have carried out $\simeq 400$ such Runs.

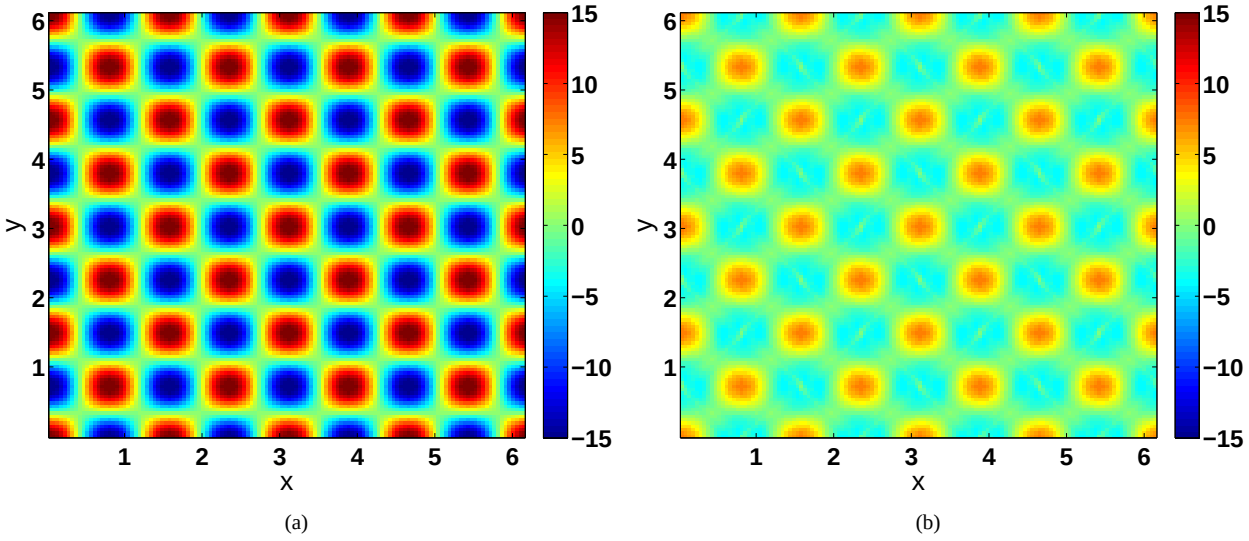

Figure 1. Pseudocolour plots of the Okubo-Weiss parameter Λ for (a) $\Omega = 1$ and $\tau_P = 0$ and (b) $\Omega = 20$ and $\tau_P = 1$; these show vortex-crystal states. Given our color bar in (a), vortical regions are red and strain-dominated regions are dark blue.

sets we calculate the quantities, such as $E(t)$, which we have defined above; and from these calculations we obtain the rich, nonequilibrium phase diagram of Fig. 3 (a), in which blue circles represent the *steady crystal* SXA, green circles represent either *temporally periodic* (OPXA) or *quasiperiodic* (OQPXA) states, and the red circles represent the state SCT that displays *spatiotemporal chaos and turbulence*. The most striking feature of this nonequilibrium phase diagram is that the boundaries between the different states are very complicated, with a fractal-type interleaving of the states SXA, OPXA/OQPXA, and SCT; this is especially clear in Fig. 3(b), which shows a detailed view of the phase diagram in the vicinity of the these boundaries. Earlier studies of elastic turbulence seem to have missed the complicated nature of these boundaries because they have not been able to examine these transition in as much detail as we have done.

Fractal-type boundaries between different nonequilibrium states have been obtained in nonequilibrium phase diagrams for some other extended dynamical systems. Examples of such boundaries can be found in the transition to turbulence in pipe flow,[40] the transitions between different spiral-wave patterns in mathematical models for cardiac tissue,[41,42] and the transition from no-dynamo to dynamo regimes in a shell model for magnetohydrodynamic (MHD) turbulence.[43] In many dynamical systems a fractal basin boundary can separate the basin of attraction of a fixed point or a limit cycle from the domain of attraction of a strange attractor; thus, a small change in the initial condition can lead either to the simple dynamical evolutions, associated with fixed points or limit cycles, or to chaos, because of a strange attractor. The 2D Navier-Stokes (NS) and FENE-P equations that we study here comprise a $4N^2$-dimensional dynamical systems, where N^2 is the number of grid points; the factor of 4 appears here because we have the 2D vorticity and the three independent components of the $\mathscr{L}$ matrix at each

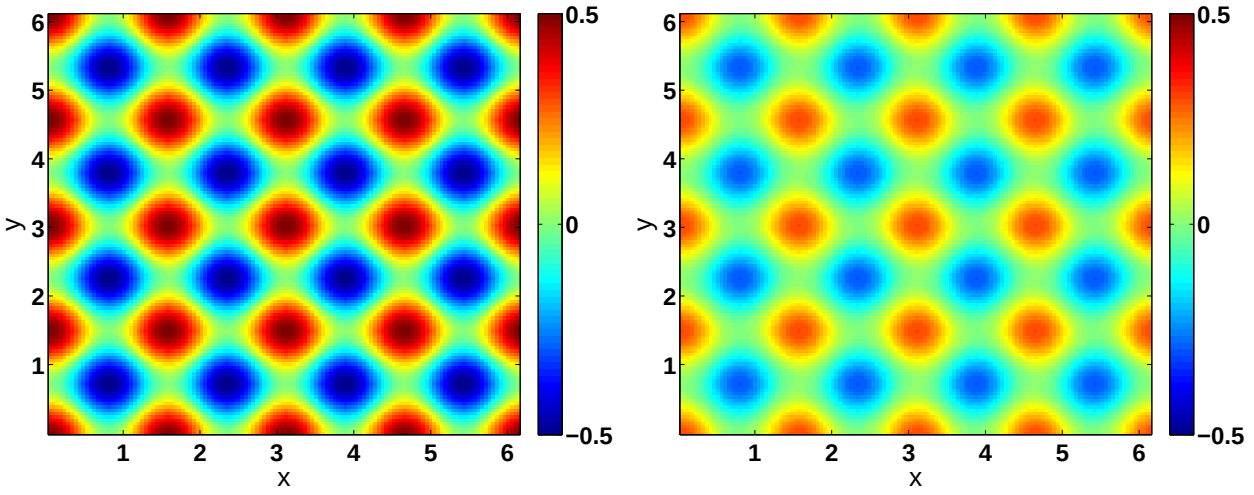

Figure 2. Pseudocolour plots of the stream function ψ, illustrating vortex-crystal states, for (a) $\Omega = 1$ and $\tau_P = 0$ and (b) $\Omega = 20$ and $\tau_P = 1$.

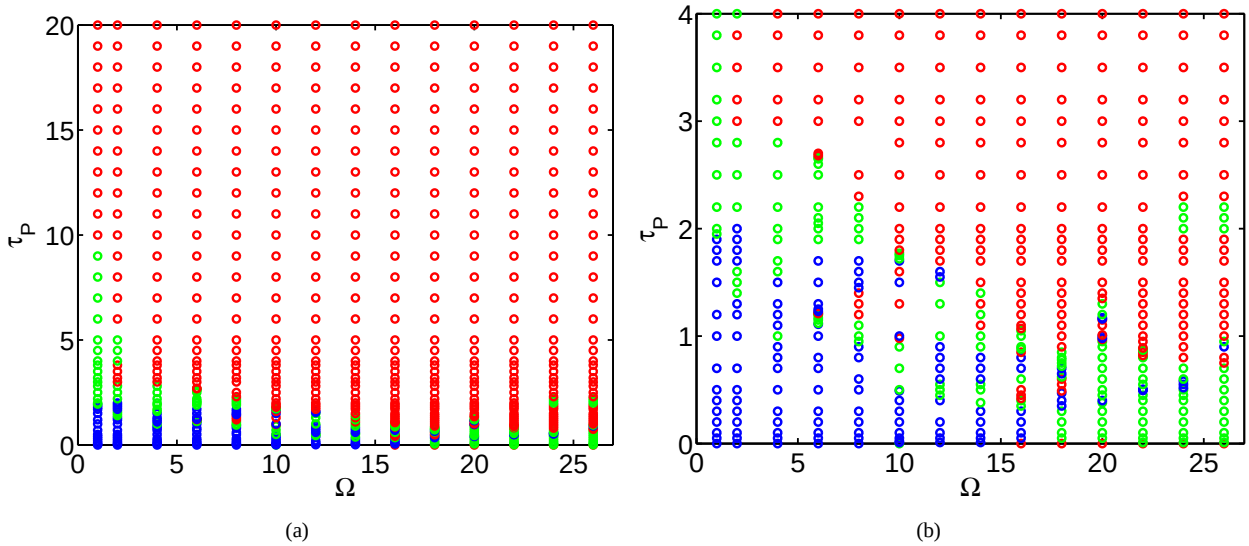

Figure 3. (a) Phase diagram of our 2D system with polymer additives in the τ_P-Ω plane, where blue circles represent the regions SX and SXA, green circles represent the regions of OPXA and OQPXA, and the red circles represents the regions of SCT; (b) an enlarged version of a region of the phase diagram in (a).

grid point. It is not feasible to find the complete basin boundaries for such a high-dimensional dynamical system (we use $N \sim 10^2$ so $4N^2 \sim 4 \times 10^4$); however, we can reasonably assume that complicated, fractal-type boundaries separate the basins of attraction of the SXA, OPXA/OQPXA, and SCT states. Note that we do not change the initial condition; instead, we change our dynamical system by changing the parameters F_{amp} and τ_P and, hence, $\mathscr{G}r$ and $\mathscr{W}i$. This change affects the long-time evolution of our 2D NS and FENE-P system as sensitively as does a change in the initial conditions because the fractal basin boundary itself changes with these parameters. Reference[40] has found such a sensitive dependence on model paramters in the transition to turbulence and the edge of chaos in pipe flow (see their Fig. 3, which shows that the border, in parameter space, between the laminar and turbulent regions is very complicated, in much the same way as the phase boundary is in our study). In Refs.,[41,42] it has been shown that the spatiotemporal evolution of spiral waves of electrical activation depends sensitively on inhomogeneities in partial-differential-equation models for ventricular tissue; changes in the positions of these

inhomogeneities in models for cardiac tissue correspond in our system to changes in parameters such as Ω and τ_P. A shell-model study of the dynamo transition in MHD has also found such a fractal boundary, separating dynamo and no-dynamo regimes, in the plane of the magnetic Reynolds number and the magnetic Prandtl number.[43]

In the next two subsections we describe in detail the results of our calculations for two representative values of Ω, namely, 1 and 22, and a range of values of τ_P (Table 1). We have carried out many such calculations ($\simeq 400$) to obtain the phase diagram of Fig. 3.

The case $\Omega = 1$

If $\Omega = 1$, which lies in region $\Omega < \Omega_{s,n=4}$, the steady-state solution is $\omega_{s,n=4}$, in the absence of polymers. When we add FENE-P polymers to the 2D Navier-Stokes fluid and increase the polymer relaxation time τ_P, the steady-state solution $\omega_{s,n=4}$ becomes unstable. For the range of values of τ_P in our runs $\mathtt{R1}-1$ (Table 1), we obtain a steady vortex crystal, which is shown by the pseudocolor plots of ψ and Λ in Figs. 4(a) and (b), respectively, for the illustrative value $\tau_P = 1$; for this set of parameters, Fig. 4(c) shows the reciprocal-space spectrum E_Λ, which has clear, dominant peaks at the forcing wave vectors.

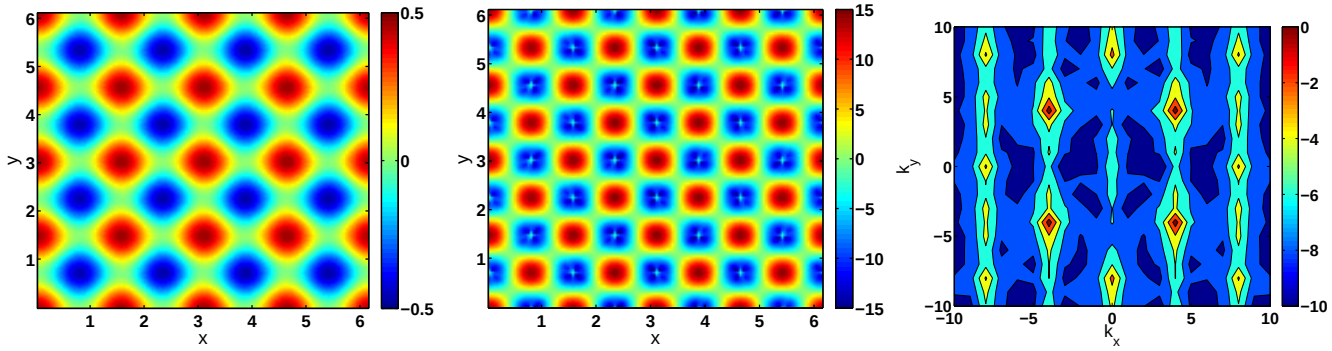

(a) (b) (c)

Figure 4. Pseudocolour plots for $\Omega = 1$ and $\tau_P = 1$: (a) the streamfunction ψ and (b) the Okubo-Weiss parameter Λ; (c) a filled contour plot of the E_Λ, reciprocal-space spectrum, this shows peaks at the forcing wave vectors.

As we increase τ_P beyond 1.9, new dynamical regimes appear in the range of values for our runs $\mathtt{R1}-2$. In particular, we observe, for $\Omega = 1$ and $\tau_P = 3$, that the time series of $E(t)$ is periodic (Fig. 5 (a)) and its power spectrum $|E(f)|$ (Fig. 5(b)) shows one dominant peak, with hardly any sign of higher harmonics. Thus, the Poincaré-type map in the $(\Re[\hat{v}(1,0)], \Im[\hat{v}(1,0)])$ plane (Fig. 5(c)) displays a simple attractor. In Figs. 5(d) and (e), we show, for these parameter values, pseudocolor plots of ψ and Λ, respectively; there is spatial undulation in the former and the latter is deformed relative to SX (Fig. 1(a)). In the reciprocal-space spectrum E_Λ (Figure 5(f)), we do not see any major peaks, other than the ones at the forcing wave vectors, because the deformation of the original is weak; however, the amplitudes of these dominants peaks are smaller than those of their counterparts, at the forcing wave vectors, in Fig.4(c).

An additional increase of τ_P (runs $\mathtt{R1}-3$ with $\tau_p > 10$) leads to chaotic temporal evolution and a disordered set of vortices and antivortices in space. Thus, we have states with spatiotemporal chaos and turbulence; for our nonequilibrium system, turbulent states with spatiotemporal chaos are the analogues of the disordered liquid state, which appears on the melting of an equilibrium crystal.[1–6] We illustrate a state with spatiotemporal chaos for $\Omega = 1$ and $\tau_P = 20$ by the plots in Fig. 6. In particular, Fig. 6(a) shows the the chaotic enery time series $E(t)$, whose power spectrum $|E(f)|$ (Fig 6(b)) shows a broad background, which indicates temporal chaos. The scattered points in the Poincaré-type section in the $(\Re[\hat{v}(1,0)], \Im[\hat{v}(1,0)])$ plane confirm the presence of chaos. The disorder of this state is shown in the pseudocolor plots of ψ and Λ in Figs. 9(d) and (e), respectively; and the associated reciprocal-space spectrum $E_\Lambda(\mathbf{k})$ (Fig. 9(f)) shows many new Fourier modes in addition to the residual peaks at the forcing wave vectors.

Thus, we see that the onset of elastic turbulence can lead to vortex-crystal melting, through a very rich sequence of transitions, even when Ω is itself too small to melt this nonequilibrium crystal. The spatial autocorrelation function $G(\mathbf{r})$ and the evolution of the order parameters $\langle \hat{\Lambda}_\mathbf{k} \rangle$ with τ_P are given in the second fifth subsection.

The case $\Omega = 22$

If we do not have any polymers and if $\Omega = 22$, which is greater than $\Omega_{s,n=4}$, the steady-state solution $\omega_{s,n=4}$ is unstable, and the temporal evolution of our system is chaotic as we can see from the time series of energy in Fig. 7(a). Its power spectrum $|E(f)|$, which is plotted in Fig. 7(b), has several peaks in a broad background, and the Poincaré-type section in the

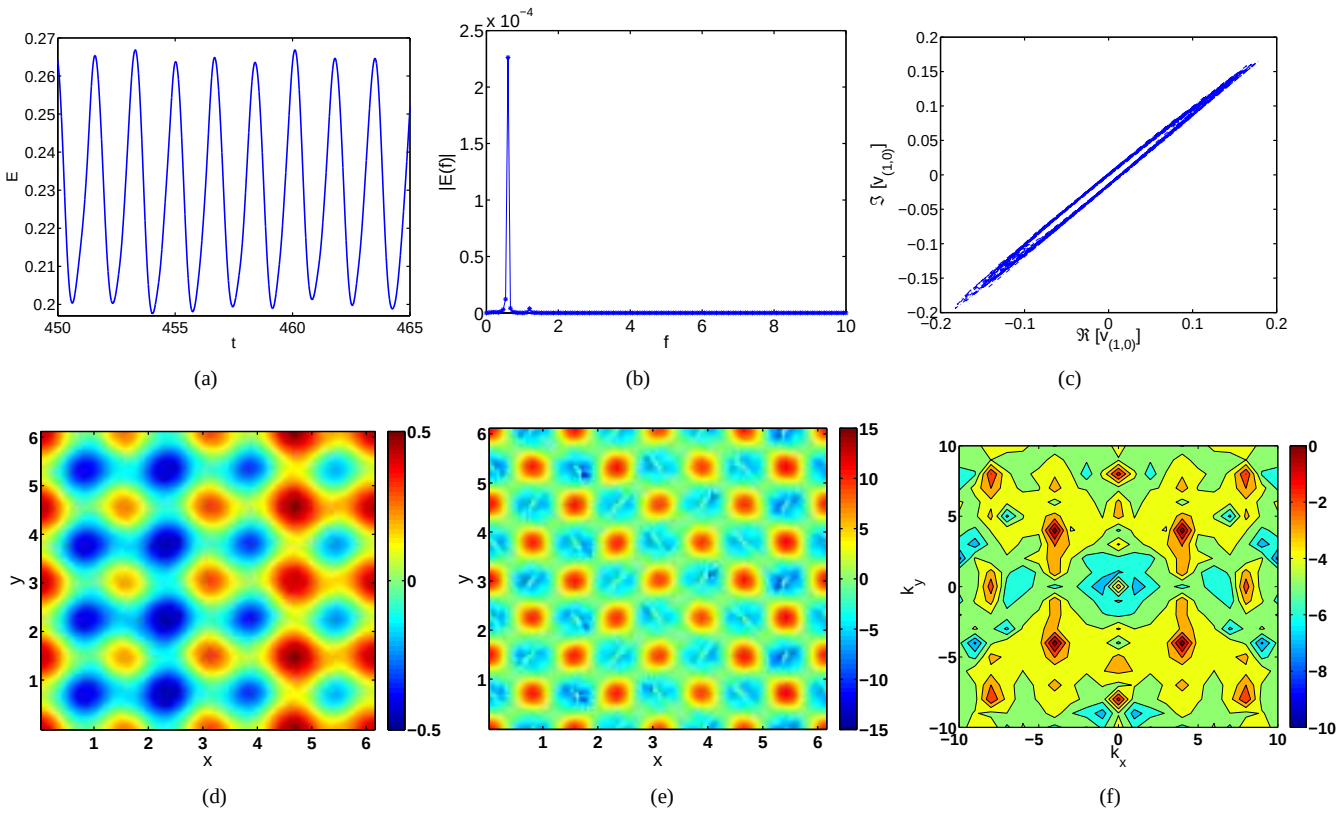

Figure 5. Plots, for $\Omega = 1$ and $\tau_P = 3$: (a) the time evolution of the energy $E(t)$, (b) its power spectrum $|E(f)|$ versus the frequency f, and (c) the Poincaré-type section in the plane $(\Re[\hat{v}(1,0)], \Im[\hat{v}(1,0)])$. Pseudocolor plots of (d) the streamfunction ψ, (e) the Okubo-Weiss parameter Λ, and (f) a filled contour plot of the reciprocal-space spectrum E_Λ; the amplitudes of the principal peaks in (f) are lower than the amplitudes of their counterparts, at the forcing wave vectors, in Fig. 4(c).

$(\Re[\hat{v}(1,0)], \Im[\hat{v}(1,0)])$ (Fig. 7 (c)) displays points that cover a two-dimensional area. The disordered spatial structure of this state, shown by the pseudocolor plots of ψ and Λ in Figs. 7 (d) and (e), respectively, indicates that this state is spatiotemporally chaotic and turbulent. Figure 7 (f) shows the reciprocal-space energy spectrum E_Λ, which exhibits a large number of Fourier modes in addition to the ones at the forcing wave vectors.

When we add polymers to our 2D Navier-Stokes system at $\Omega = 22$, these polymers lead first to a reappearance of states that are periodic in time; this occurs, e.g., for the range of τ_p covered in runs $\mathtt{R}22-2$. For $\tau_p = 0.3$, Fig. 8(a) shows that time series of the energy is periodic in time and its power spectrum $|E(f)|$ (Fig. 8(b)) has a fundamental peak at $f_0 = 2.5 \times 10^{-3}$ and harmonics at $f_1 = 2f_0$, $f_2 = 3f_0$, $f_4 = 4f_0$, and $f_5 = 5f_0$. The Poincaré-type section in the $(\Re[\hat{v}(1,0)], \Im[\hat{v}(1,0)])$ plane in Fig. 8 (c) exhibits a simple attractor, which is consistent with the periodic behaviors that emerge from Figs. 8(a) and (b). The spatial organization of this state, shown by pseudocolor plots of ψ and Λ in Figs. 8 (d) and (e), respectively, is disordered, although some vestiges of the unit cells of the original crystal are visible in the pseudocolor plot of Λ; and Fig. 8 (f) shows the reciprocal-space spectrum E_Λ.

If we increase the polymer relaxation time to $\tau_P = 0.5$ in run $\mathtt{R}22-3$, we obtain a new steady state that is a vortex crystal; however, it is not exactly the same as the original vortex crystal as can be seen clearly by comparing the pseudocolor plots of Λ in Figs. 1(a) and 9(b). This difference is even more striking if we compare the pseudocolor plots of ψ shown in Figs. 9(a) and 2(a) and. Not surprisingly, then, the reciprocal-space energy spectrum E_Λ, shows new peaks in addition to the ones at the forcing wave vectors, which now appear with a reduced amplitude.

If we increase τ_p some more (runs $\mathtt{R}22-4$ with $0.55 \leq \tau_P \leq 0.8$), we obtain a spatiotemporal crystal, i.e., one that is spatially periodic and which also oscillates in time.[6] For instance, if $\tau_P = 0.7$, the time series of the energy is periodic in time, as shown in Fig. 10(a); and Fig. 10(b) shows that its power spectrum $|E(f)|$ has only one dominant peak, which is a clear indication that temporal evolution is periodic. Figure 10(c) shows the Poincaré-type section in the $(\Re[\hat{v}(1,0)], \Im[\hat{v}(1,0)])$ plane, which displays that the projection of the attractor on this plane is a closed loop. Figures 10(d) and (e) show pseudocolor

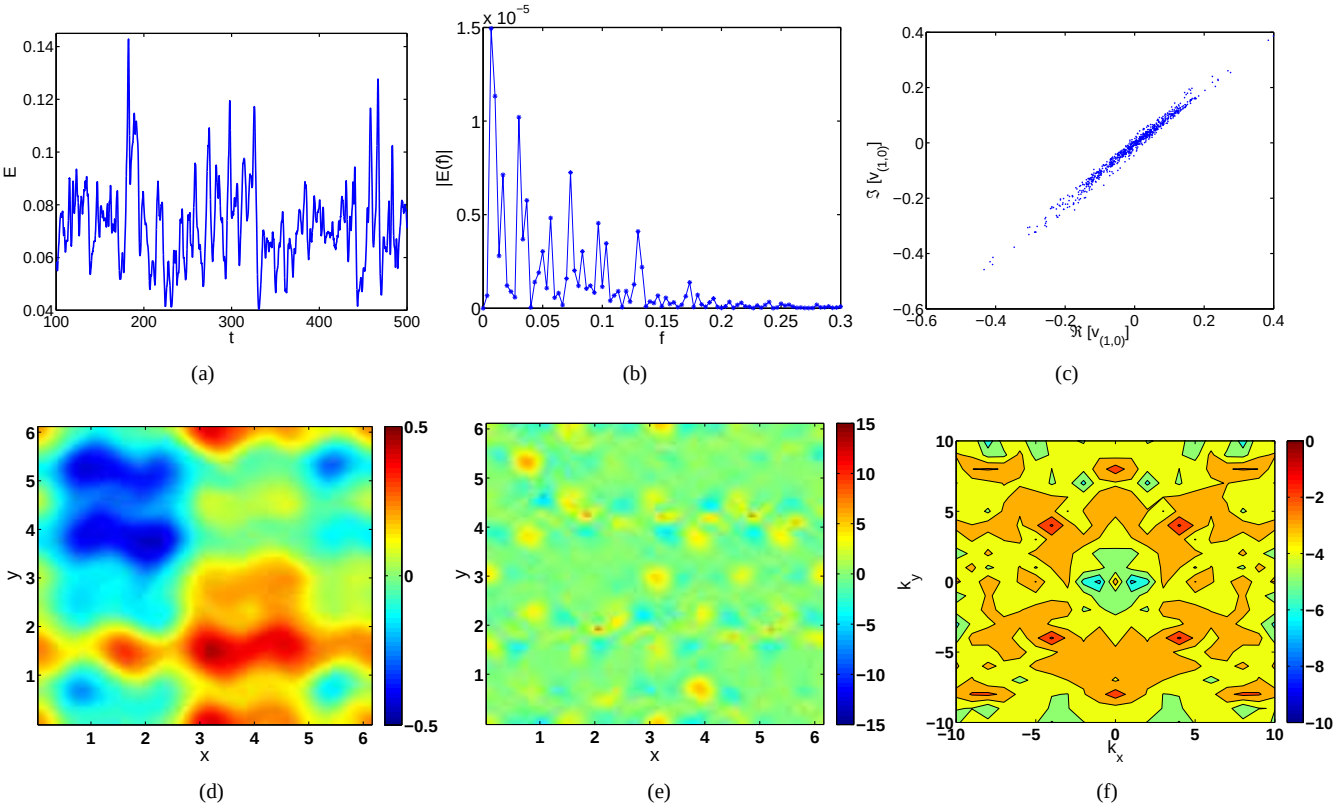

Figure 6. Plots for $\Omega = 1$ and $\tau_P = 20$: (a) the time evolution of the energy $E(t)$, (b) its power spectrum $|E(f)|$ versus the frequency f, and (c) the Poincaré-type section in the plane $(\Re[\hat{v}(1,0)], \Im[\hat{v}(1,0)])$. Pseudocolour plots of (d) the streamfunction ψ and (e) the Okubo-Weiss parameter Λ; and (f) a filled contour plot of the reciprocal-space spectrum E_Λ, which shows that various Fourier modes are present in addition to those at the forcing wave vectors.

plot of ψ and Λ, respectively; and the associated reciprocal-space spectrum E_Λ (Fig. 10(f)) shows dominant peaks principally at the forcing wave vectors.

We now increase τ_P a little more (run $\mathtt{R22-5}$); the temporal evolution of the system becomes chaotic and the spatial organization of the vortex crystal is distorted. Thus, we finally enter a state with spatiotemporal chaos and turbulenc (SCT); this is our analogue of the disordered, liquid state, which appears on the melting of an equilibrium crystal.[1,3–5] However, some vestiges of the incipient crystalline ordering can still be found in reciprocal-space spectra, as we illustrate for $\tau_P = 20$ in Fig. 11. From the time series $E(t)$ of the energy (Fig. 11(a)), it is clear that system is chaotic; this is confirmed by the power spectrum $|E(f)|$ (Fig. 11(b)), which displays several peaks, and the Poincaré-type section in the $(\Re[\hat{v}(1,0)], \Im[\hat{v}(1,0)])$ plane (Fig. 11(c)), in which the points fill a two-dimensional area. The disordered spatial organization of vortical structures is shown in Figs. 11(d) and (e) via pseudocolor plots of ψ and Λ, respectively. The reciprocal-space spectrum $E_\Lambda(k)$ (Fig. 11(f)) shows residual peaks at the forcing wave vectors, which indicate the incipient vortex crystal, but the other Fourier modes show that long-range spatial periodicity has been lost in this SCT state.

Thus, our careful study of the case $\Omega = 22$ for various values of τ_P shows how the turbulent SCT state, at $\tau_P = 0$, gives way to the states OPXA, SXA, and OPXA states, as we increase τ_P (Table 1); finally these states show reentrant melting into the SCT state.

Order Parameters, Spatial Correlation Functions, and Kinetic Energy Spectra

We now use statistical measures that are employed in the density-functional theory[1,3–5] of freezing. In particular, we examine the dependence of the order parameters $\langle\hat{\Lambda}_{\mathbf{k}}\rangle$ and the spatial autocorrelation function $G(\mathbf{r})$, defined in Eq. (4), on τ_P and Ω. Recall that equilibrium melting is a first-order transition at which $\rho_{\mathbf{G}}$ jumps discontinuously from a nonzero value in the crystal to zero in the liquid. The melting of our nonequilibrium vortex crystal is far more complicated, in all parts of the parameter space of the phase diagram of Fig. 3, because there are many transitions.

For our nonequilibrium vortex crystal $\Re\langle\hat{\Lambda}_{\mathbf{k}}\rangle$, which is obtained by summing $\hat{\Lambda}_{\mathbf{k}}$ over the four forcing wave vectors, is

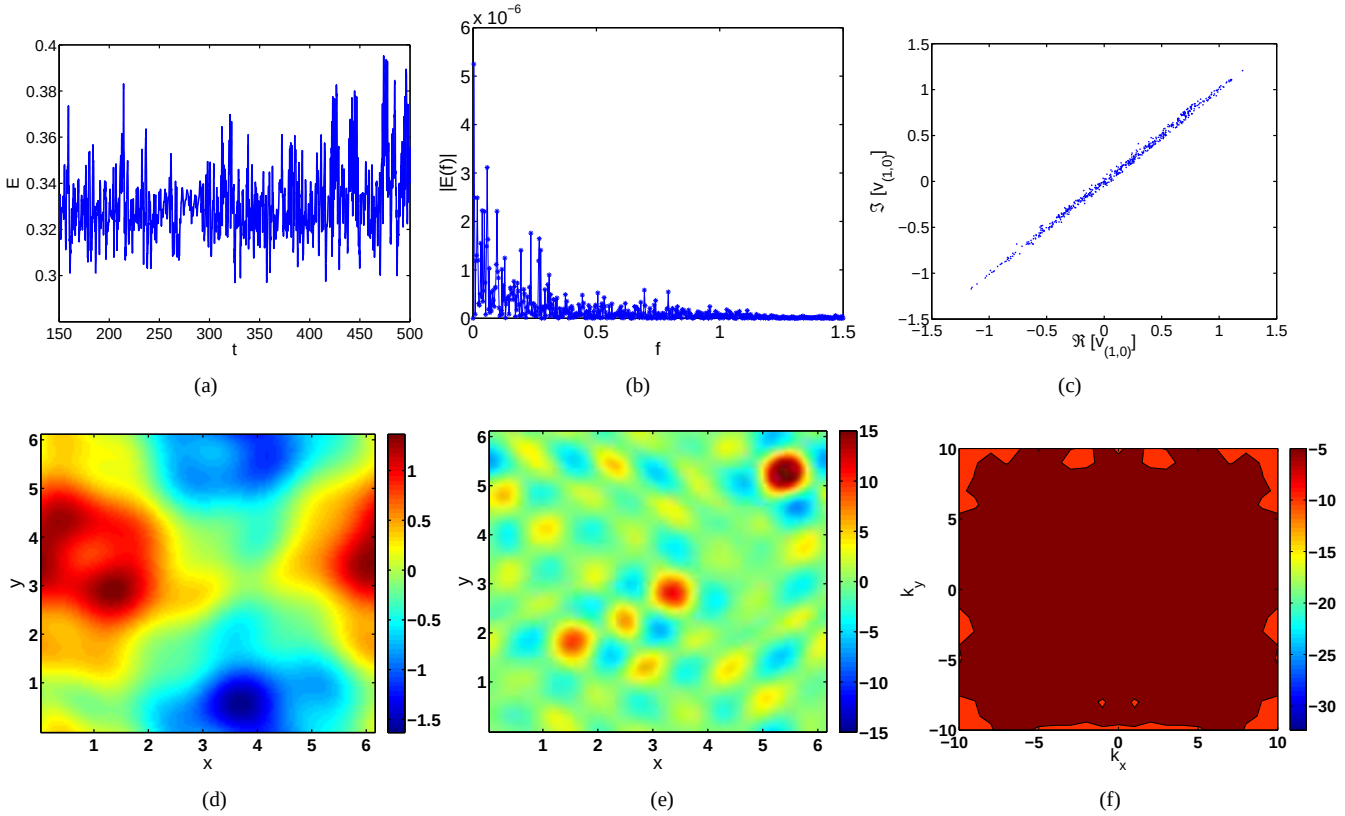

Figure 7. Plots for $\Omega = 22$ and $\tau_P = 0$: (a) the time evolution of the energy $E(t)$ (b) its power spectrum $|E(f)|$ versus the frequency f, and (c) the Poincaré-type section in the plane $(\Re[\hat{v}(1,0)], \Im[\hat{v}(1,0)])$. Pseudocolor plots of (d) the streamfunction ψ and (e) the Okubo-Weiss parameter Λ; and (f) a filled contour plot of the reciprocal-space spectrum E_Λ, which show a large number of Fourier modes in addition to the ones at the forcing wave vectors.

the analogue of the order parameters $\Re\langle\rho_{\mathbf{G}}\rangle$ in a conventional crystal. $\Re\langle\hat{\Lambda}_{\mathbf{k}}\rangle$ changes with τ_P as shown, respectively, for (a) $\Omega = 1$ and $\mathbf{k} = (4,4)$ and (b) $\Omega = 22$ and $\mathbf{k} = (4,4)$ in Figs. 12 (a) and (b). For $\Omega = 1$ and small values of τ_p, the steady state of our system is SX, so the Fourier modes at the forcing wave vector are the most significant ones. As we increase τ_p, our nonequilibrium system undergoes a series of transitions from SX to the turbulent state SCT (see above); therefore, $\Re\langle\hat{\Lambda}_{\mathbf{k}}\rangle$ decreases with τ_P as we show in Fig. 12(a). For $\Omega = 22$ and $\tau_p = 0$, we begin with a system that is disordered and turbulent; if we then increase τ_P, our system first goes to the state SX, so $\Re\langle\hat{\Lambda}_{\mathbf{k}}\rangle$ first increases as we show in Fig. 12(b); as we increase τ_p, the system becomes turbulent and disordered again, so $\Re\langle\hat{\Lambda}_{\mathbf{k}}\rangle$ decreases at large τ_P (Fig. 12(b)).

We give representative plots of the correlation function $G(\mathbf{r})$ (see Eq.(4)) in Figs. 13 (a)-(d). For the crystal, we calculate $G(\mathbf{r})$ along the line from $\mathbf{r} = (\pi/2, \pi/2)$ and $\mathbf{r} = (\pi/2, \pi)$; this shows periodic peaks [Figs. 13 (a) for $\Omega = 1, \tau_P = 1$] with widths are related to those of vortical or strain-dominated regions. In the turbulent phase we use a circular average of G [Figs. 13 (b), (c), and (d) for $\Omega = 1$ and $\tau_P = 20$, $\Omega = 22$ and $\tau_P = 0$, and $\Omega = 22$ and $\tau_P = 20$, respectively]; these peaks decay over a length scale that yields the degree of short-range order. This decay is similar to the decay of spatial correlation functions in a disordered liquid phase in an equilibrium system.

We have also obtained the energy spectra $E(k)$ in two parts of the turbulent state of our system; the first part is dominated by elastic turbulence and the other one lies in the region of fluid turbulence, where polymers lead to dissipation reduction. For a given resolution, there is one qualitative difference between the energy spectra in these two regimes. In the forward-cascade part of $E(k)$, the slope of the energy spectrum is higher in the elastic-turbulence regime than in the dissipation-reduction regime as we show in Fig. 14 (a), for $\Omega = 4$ and $\tau_P = 10$ (red line), $\Omega = 4$ and $\tau_P = 40$ (green line), and $\Omega = 50$ and $\tau_P = 5$ (black line). We have also obtained the spectrum of polymer stretching, which is defined as $[Tr(C)](k) \equiv \sum_{k-1/2<k'\leq k+1/2} k'^2 \langle |\widehat{C_{11}}(\mathbf{k}',t)|^2 + \widehat{C_{22}}(\mathbf{k}',t)|^2\rangle_t$, where $\langle\rangle_t$ denotes a time average over the statistically steady state. In Fig. 14 (b) we show the polymer-stretching spectra, for $\Omega = 4$ and $\tau_P = 10$ (red line), $\Omega = 4$ and $\tau_P = 40$ (green line), and $\Omega = 50$ and $\tau_P = 5$ (black line).

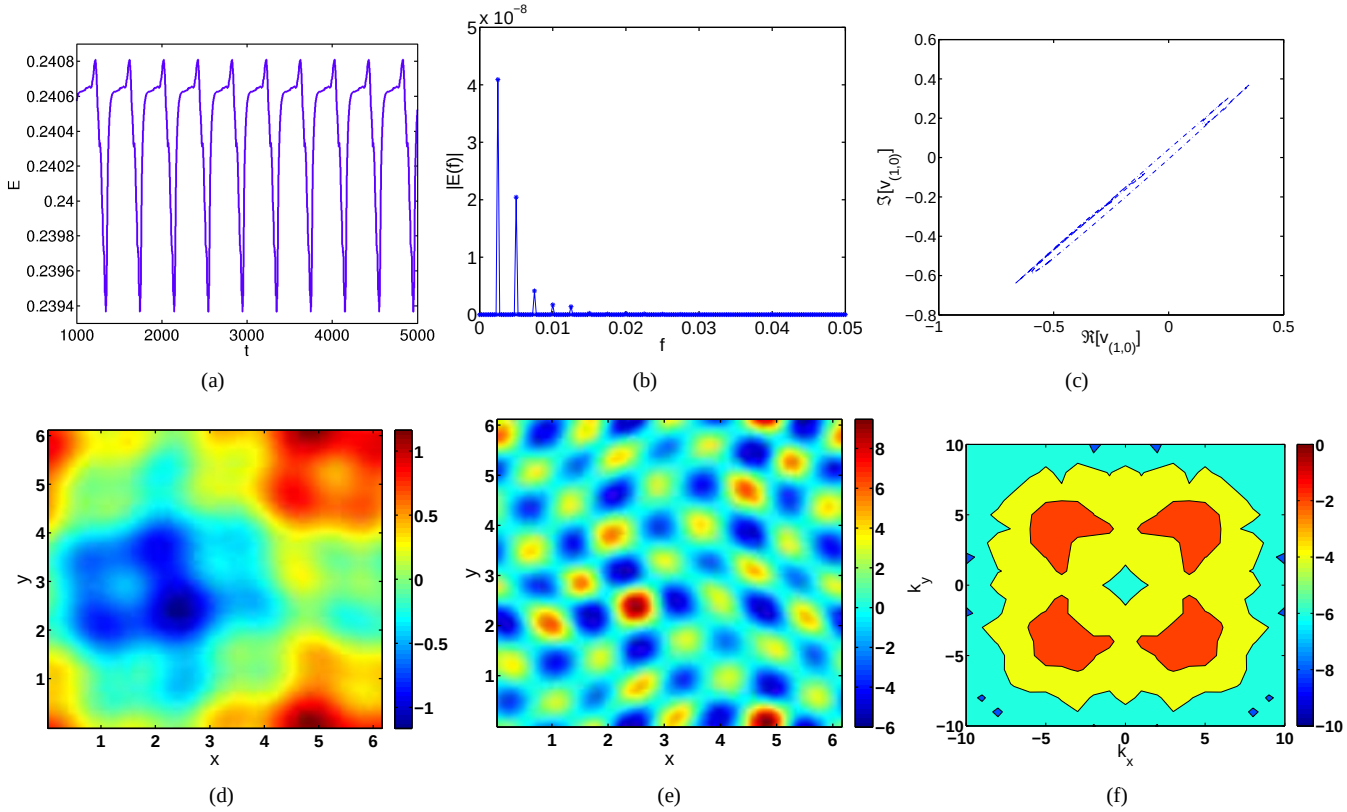

Figure 8. Plots for $\Omega = 22$ and $\tau_P = 0.3$: (a) the time evolution of the energy $E(t)$, (b) the power spectrum $|E(f)|$ versus the frequency f, (c) the Poincaré-type section in the plane $(\Re[\hat{v}(1,0)], \Im[\hat{v}(1,0)])$. Pseudocolour plots of (d) the streamfunction ψ and (e) the Okubo-Weiss parameter Λ; (f) a filled contour plot of the reciprocal-space spectrum E_Λ.

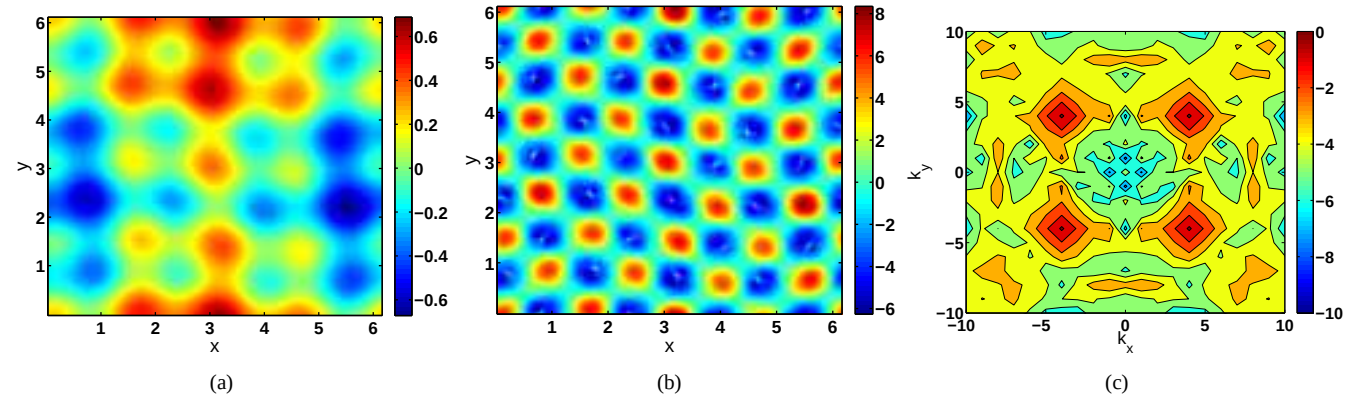

Figure 9. Pseudocolor plot for $\Omega = 22$ and $\tau_P = 0.5$: (a) the streamfunction ψ and (b) the Okubo-Weiss parameter Λ; and (c) a filled contour plot of the reciprocal-space spectrum E_Λ, which shows peaks at the forcing wave vectors, but with amplitudes that are lower than for their counterparts in Fig.4(c).

Spatial Patterns of Polymers and Inertial Particles in our Nonequilibrium System

It is instructive to study the spatial patterns of polymers and inertial particles in the nonquilibrium states of our system; we show below that such patterns also provide clear signatures of these states. In Figs. 15 (a), (b), (c), and (d) we show contours of the polymer stretching r_P^2 superimposed on pseudocolor plots of the Okubo-Weiss field Λ for $\Omega = 1$ and $\tau_P = 1$ (crystalline state), $\Omega = 1$ and $\tau_P = 20$ (melted crystal in the elastic-turbulence regime), $\Omega = 22$ and $\tau_P = 0.5$ (frozen crystal), and $\Omega = 22$ and $\tau_P = 20$ (melted crystal in the dissipation-reduction regime), respectively. As we have seen in Ref,[14] the polymers stretch

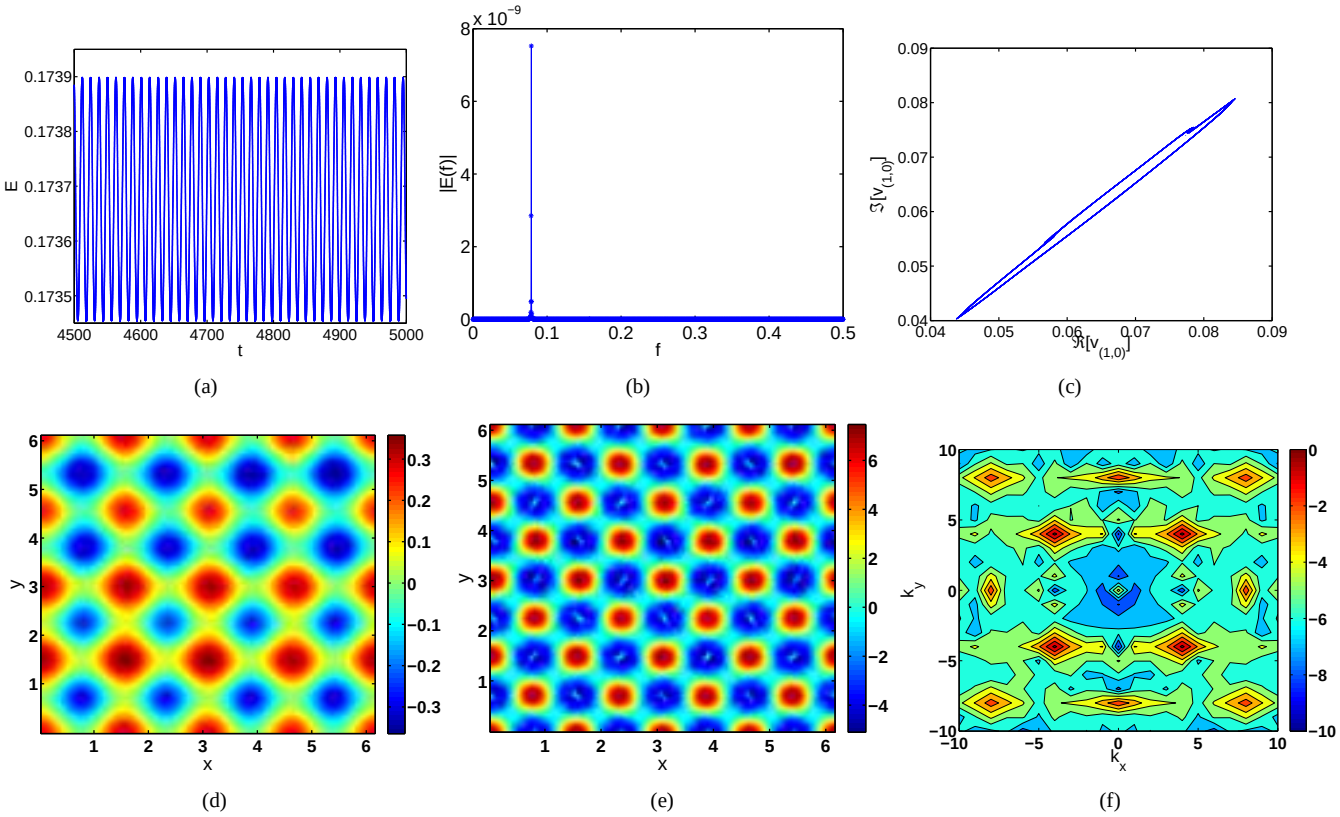

Figure 10. Plots for $\Omega = 22$ and $\tau_P = 0.7$: (a) the time evolution of the energy $E(t)$, (b) the power spectrum $|E(f)|$ versus the frequency f, (c) the Poincaré-type section in the plane $(\Re[\hat{v}(1,0)], \Im[\hat{v}(1,0)])$. Pseudocolour plots of (d) the streamfunction ψ and (e) the Okubo-Weiss parameter Λ; and (f) a filled contour plot of the reciprocal-space spectrum E_Λ.

preferentially in extensional regions, where $\Lambda < 0$; thus, the patterns of their extension mirror the spatial periodicity or lack thereof in the crystalline and turbulent phases, respectively. The spatiotemporal evolution of the plots in Fig. 15 is given in Video crystal-rp-a, b, c, and d at http://www.physics.iisc.ernet.in/∼rahul/movies.html .

The analogs of Figs. 15 (a), (b), (c), and (d), with polymers replaced by inertial particles (black dots), are given in Figs. 16 (a), (b), (c), and (d), respectively. We see from these plots that inertial particles organize themselves in regions where $\Lambda \simeq 0$; thus, their spatial organization can also be used to sumrise the underlying periodicity of a nonequilibrium vortex crystal. This method of visualization has been used in experiments on fluid films without polymers.[10,11] All these plots are for Stokes number $\mathrm{St} \approx 1$.

The analogs of Figs. 16 (a), (b), (c), and (d), with the Λ field replaced by polymers, are given in Figs. 17 (a), (b), (c), and (d), respectively. We see from these plots that the correlation between the spatial organizations of polymers and inertial particles is not dramatic. This is not surprising in so far as the polymers stretch preferentially where $\Lambda < 0$ whereas inertial particles tend to cluster in regions where $\Lambda \simeq 0$.

Conclusions

Our detailed DNS elucidates the nature of melting of a vortex crystal in a nonequilibrium forced, thin fluid film with polymer additives. This melting can be induced by (a) elastic turbulence at low Reynolds numbers Re (or Ω) but large Weissenberg numbers $\mathscr{W}i$ (or τ_P), (b) fluid turbulence at low τ_P but large Ω, or (c) a combination of these two types of turbulence (see Figs. 3 (a) and (b)). Our work leads to the rich, nonequilibrium phase diagram of Fig. 3. The topology of this phase diagram and the intricate natures of the boundaries between the different phase in it have neither been anticipated nor been studied hitherto.

Our work builds on the DNS study of Ref.,[6] which uses ideas from the density-functional theory of freezing,[1,3–5] nonlinear dynamics, and turbulence to characterize the phases and transitions in the melting, by turbulence, of a nonequilibrium vortex crystal in a 2D fluid film. Most studies of the turbulence-induced melting of a vortex crytal in a fluid film do not include

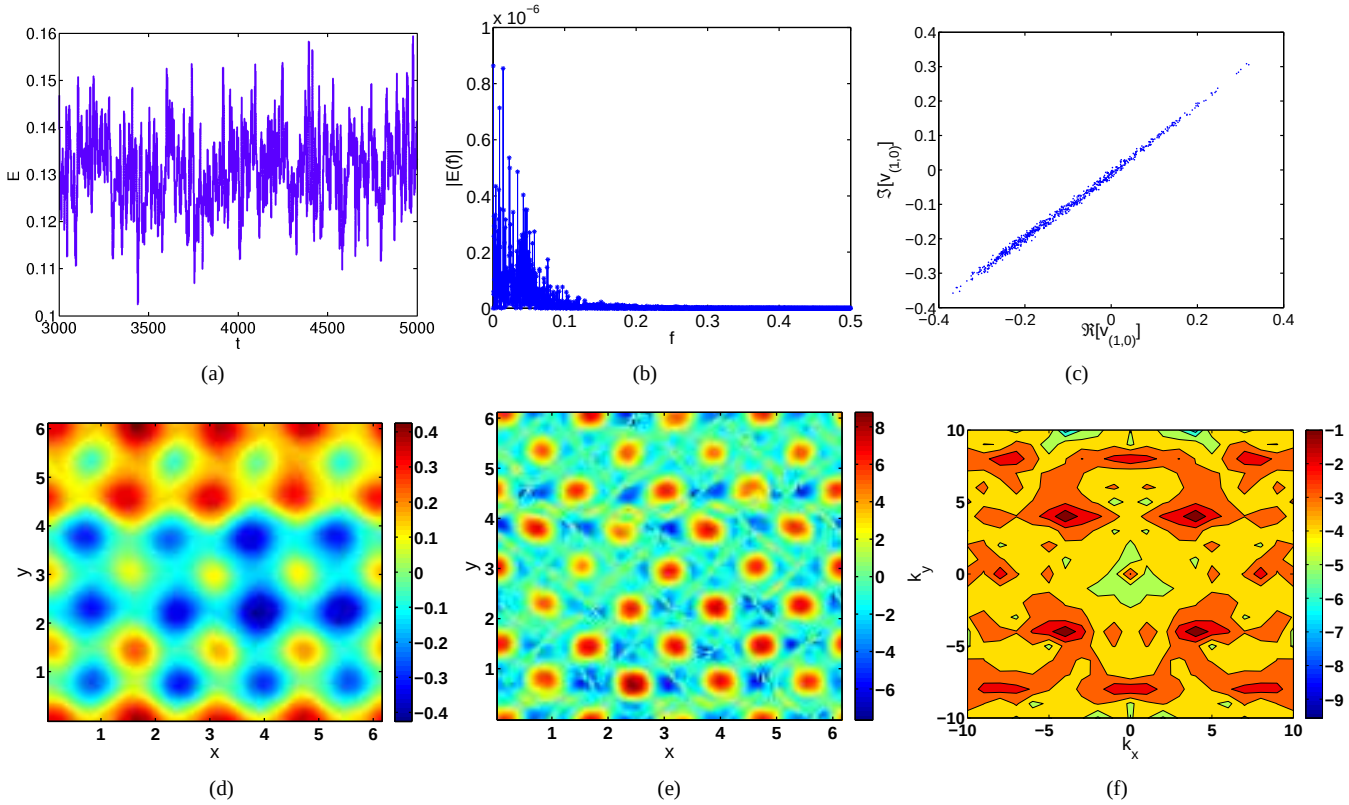

Figure 11. Plots for $\Omega = 22$ and $\tau_P = 20$: (a) the time evolution of the energy $E(t)$, (b) the power spectrum $|E(f)|$ versus the frequency f, (c) the Poincaré-type section in the plane $(\Re[\hat{v}(1,0)], \Im[\hat{v}(1,0)])$. Pseudocolour plots of (d) the streamfunction ψ and (e) the Okubo-Weiss parameter Λ; and (f) a filled contour plot of the reciprocal-space spectrum E_Λ.

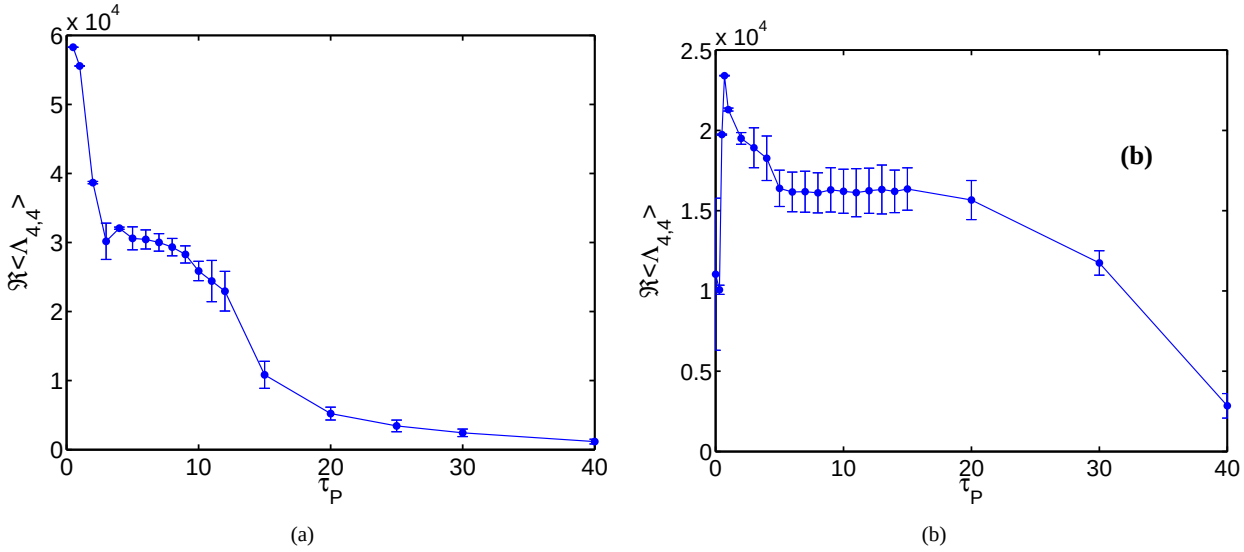

Figure 12. Plots of $\langle \hat{\Lambda}_{\mathbf{k}=(4,4)} \rangle$ versus τ_P for (a) $\Omega = 1$ and for (b) $\Omega = 22$; in (b) $\langle \hat{\Lambda}_{4,4} \rangle$ first increases with τ_P, goes through a maxima, which corresponds to an OPXA state, and then decreases after that.

polymer additives; for an overview of such studies we refer the reader to Ref.[6] The DNS study of 2D fluid films with polymer additives,[14,21,22] which uses the Oldroyd-B model, is an exception; it has studied the elastic-turbulence-induced melting of spatially periodic Kolmogorov-flow pattern, which is, in our terminology, a one-dimensional crystal. To the best of our

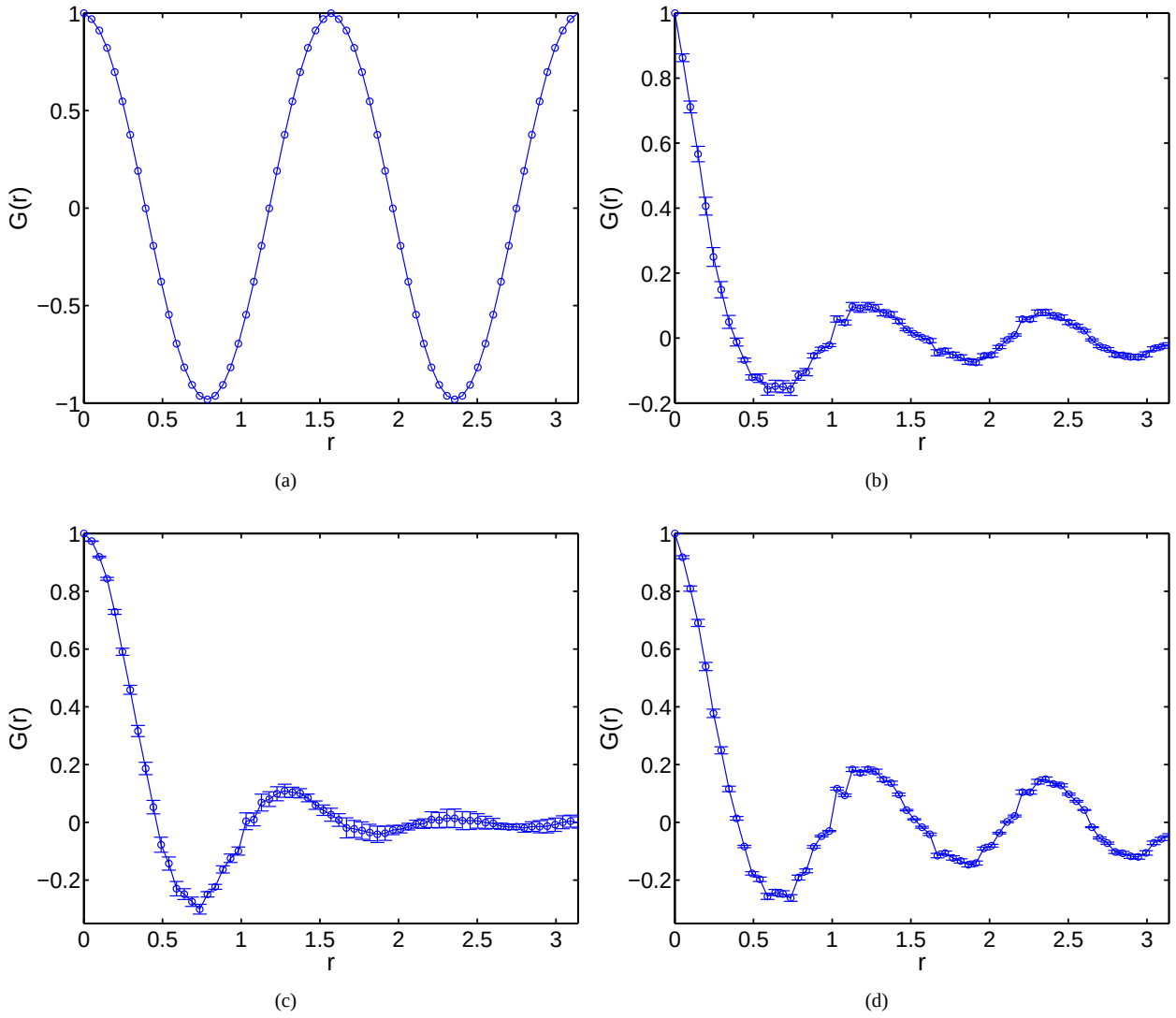

Figure 13. (a) Plot of $G(\mathbf{r})$ for the crystalline state with $\Omega = 1$ and $\tau_P = 1$ along the line connecting $\mathbf{r} = (\pi/2, \pi/2)$ and $\mathbf{r} = (\pi/2, \pi)$; and plots of the circularly averaged $G(\mathbf{r})$ in the turbulent state with (b) $\Omega = 1$ and $\tau_P = 20$, (c) $\Omega = 22$ and $\tau_P = 0$, and (d) $\Omega = 22$ and $\tau_P = 20$.

knowledge, there is no study of vortex crystals in fluid films with polymers, which brings together the variety of methods we use to analyse the melting of such crystals.

We follow Ref.,[6] which does not include polymers, in (a) identifying the order parameters for the vortex crystal, (b) characterizing the series of transitions in terms of their ψ and Λ, the energy time series $E(t)$, and their Fourier transforms, and (c) using the spatial correlation functions G in crystalline and turbulent phases. However, we go considerably beyond the study of Ref.[6] by including polymers and, therefore, (a) a new dimensionless control parameter, the Weissenberg number Wi (or τ_P), (b) the polymer-conformation tensor field $\mathscr{C}$, and (c) inertial particles. Therefore, we can examine the nonequilibrium phase diagram of this system in a two-dimensional parameter space (see Figs. 3 (a) and (b)) and elucidate the organization of polymers and inertial particles in the flow, both in crystalline and turbulent phases. We show also that our system provides a natural laboratory in which we can study the crossover from elastic-turbulence to dissipation-reduction regimes in the turbulent phase.

We refer the reader to Ref.[6] for a discussion of the thermodynamic limit and finite-size effects in such systems of nonequilibrium, vortex crystals. No study (including ours) has addressed these issues because for large system sizes, we need very large DNSs to characterize the temporal evolution of the system. If we extract a correlation length from the correlation function G, it is much smaller than the linear size of our simulation domain in the turbulent phase (SCT), so our results should

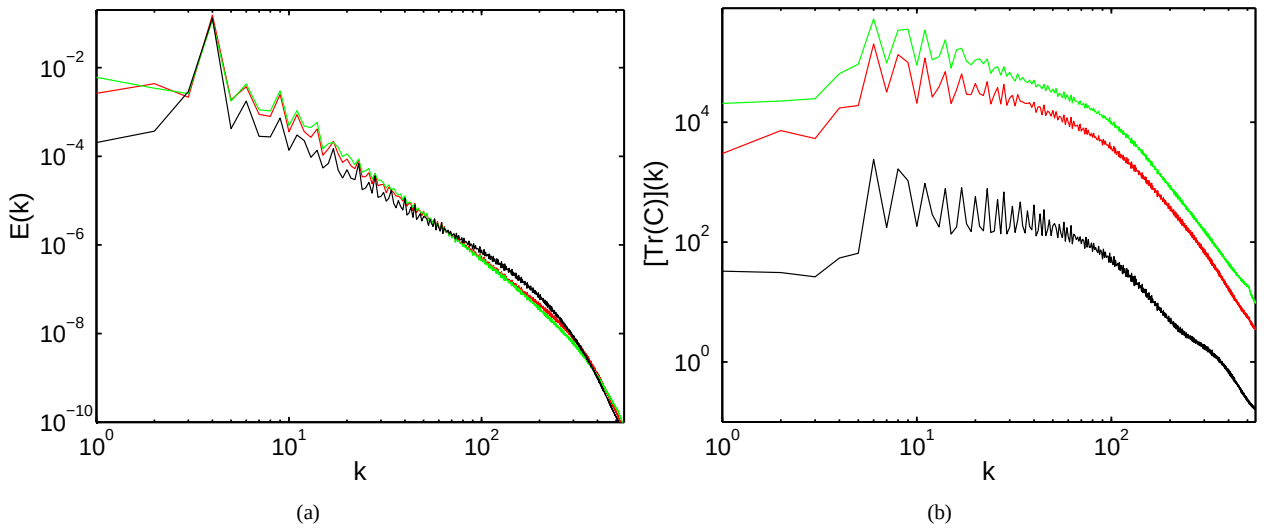

(a) (b)

Figure 14. Plots of (a) energy spectra $E(k)$ versus k and (b) polymer stretching spectra $[\mathrm{Tr}\mathscr{C}](k)$ versus k, for $\Omega = 4$ and $\tau_P = 10$ (red line), $\Omega = 4$ and $\tau_P = 40$ (green line), and $\Omega = 50$ and $\tau_P = 5$ (black line).

not change if we increase the system size. However, subtle size dependence might occur in the ordered phase because of the inverse cascade, well known in 2D fluid turbulence, which might lead to undulations that give rise to crystals with ever larger unit cells, whose size can be controlled only by the inclusion of friction. A systematic study of such subtle finite-size effects lies beyond the scope of our study.

The sequence of transitions that take us from a vortex crystal to the turbulent state is far richer than conventional equilibrium melting. The former differ from the latter in another important way: To maintain the steady states, statistical or strictly steady, we must impose the force F_ω; in the language of phase transitions, this force is a symmetry-breaking field, both in the ordered and disordered phases. Therefore, there is no symmetry difference between the disordered, turbulent state and the ordered vortex crystal, as we see directly from the vestiges of the dominant peaks in the reciprocal-space spectra $E_\Lambda(\mathbf{k})$; and the order parameters $\langle\hat{\Lambda}_\mathbf{k}\rangle$, with $\mathbf{k} = (4,4)$ the forcing wave vectors, do not become exactly zero in the turbulent phase; however, they do become very small. Moreover, our nonequilibrium vortex crystal undergoes a sequence of transitions from an ordered state to an undulating crystal and then to a fully turbulent state; there is no external or thermal noise here and hence no fluctuations in the perfect vortex crystal; this has no equilibrium analogue.

We hope that our study will encourage experimental groups to try to obtain the rich phase diagram of the melting of a nonequilibrium vortex crystal in a fluid film with polymer additives. We have recently learnt of a Shell-model study of elastic turbulence that is being prepared for publication.[44]

Acknowledgments

We thank CSIR, UGC, and DST (India) for support, SERC (IISc) for computational resources, and P.Perlekar, D. Mitra, S.S. Ray, and D. Vincenzi for discussions. AG kindly acknowledges funding from the European Research Council under the Europeans Community's Seventh Framework Programme (FP7/2007-2013)/ERC Grant Agreement N. 297004

References

1. Ramakrishnan, T. & Yussouff, M. First-principles order-parameter theory of freezing. Physical Review B **19**, 2775 (1979).
2. Haymet, A. Theory of the equilibrium liquid-solid transition. Annual Review of Physical Chemistry **38**, 89–108 (1987).
3. Chaikin, P. M. & Lubensky, T. C. Principles of condensed matter physics, vol. 1 (Cambridge Univ Press, 2000).
4. Oxtoby, D. Liquids, freezing and glass transition. Les Houches Summer School Lectures vol LI (1991).
5. Singh, Y. Density-functional theory of freezing and properties of the ordered phase. Physics Reports **207**, 351–444 (1991).

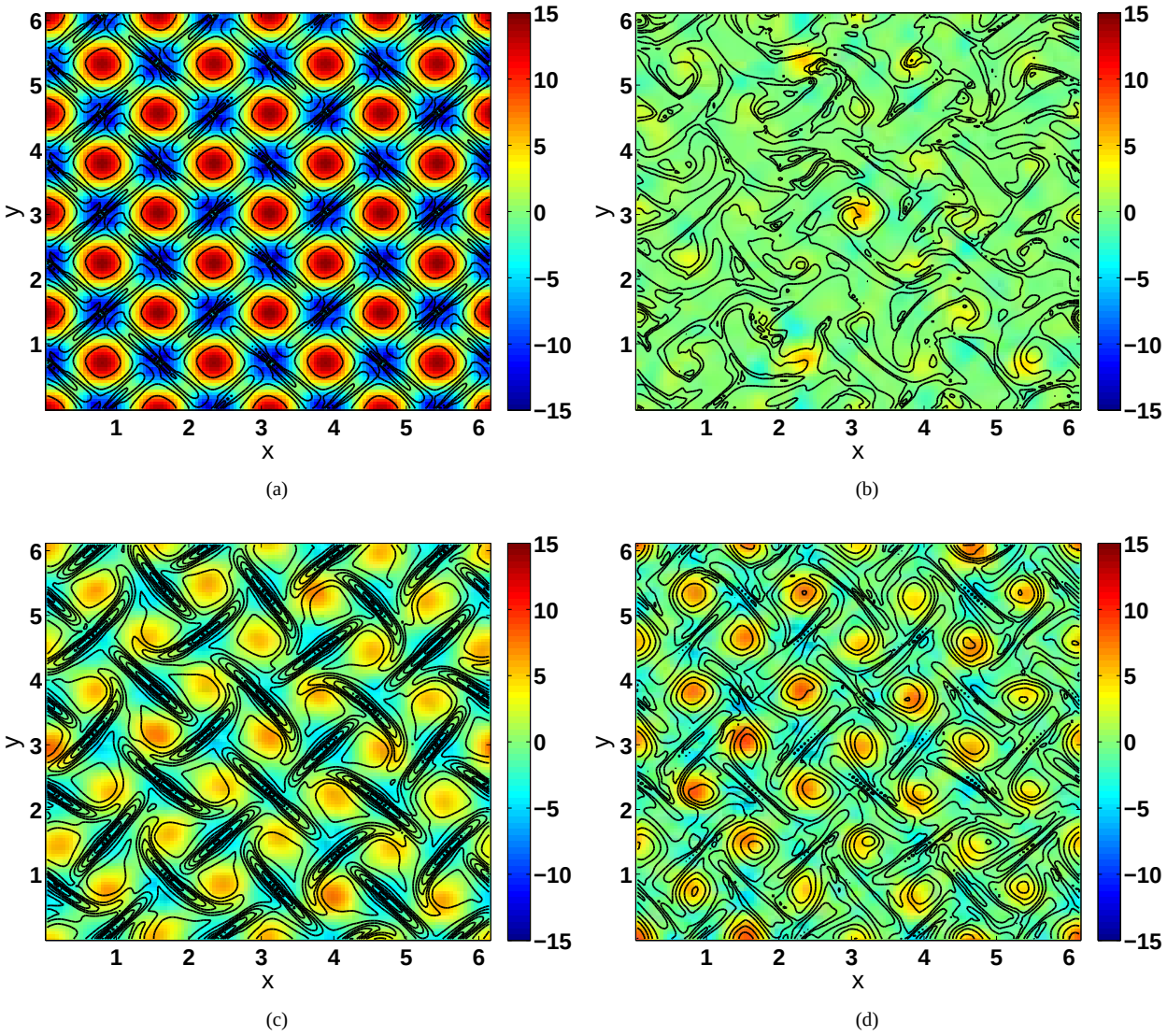

Figure 15. Plots of contours of polymer stretching r_P^2 superimposed on a pseudocolor plot of the Okubo-Weiss field Λ for (a) $\Omega = 1$ and $\tau_P = 1$ (crystalline phase), (b) $\Omega = 1$ and $\tau_P = 20$ (melted crystal in the elastic-turbulence regime), (c) $\Omega = 22$ and $\tau_P = 0.5$ (frozen crystal), and (d) $\Omega = 22$ and $\tau_P = 20$ (melted crystal in the dissipation-reduction regime).

6. Perlekar, P. & Pandit, R. Turbulence-induced melting of a nonequilibrium vortex crystal in a forced thin fluid film. New Journal of Physics **12**, 023033 (2010).

7. Das, M., Ramaswamy, S. & Ananthakrishna, G. Melting-freezing cycles in a relatively sheared pair of crystalline monolayers. EPL (Europhysics Letters) **60**, 636 (2002).

8. Gotoh, K. & Yamada, M. Instability of a cellular flow. Physical Society of Japan, Journal **53**, 3395–3398 (1984).

9. Gotoh, K. & Yamada, M. The instability of rhombic cell flows. Fluid dynamics research **1**, 165–176 (1987).

10. Ouellette, N. T. & Gollub, J. P. Curvature fields, topology, and the dynamics of spatiotemporal chaos. Physical Review Letters **99**, 194502 (2007).

11. Ouellette, N. T. & Gollub, J. P. Dynamic topology in spatiotemporal chaos. Physics of Fluids **20**, 064104–064104 (2008).

12. Perlekar, P., Mitra, D. & Pandit, R. Direct numerical simulations of statistically steady, homogeneous, isotropic fluid turbulence with polymer additives. Physical Review E **82**, 066313 (2010).

13. Perlekar, P., Mitra, D. & Pandit, R. Manifestations of drag reduction by polymer additives in decaying, homogeneous, isotropic turbulence. Physical Review Letters **97**, 264501 (2006).

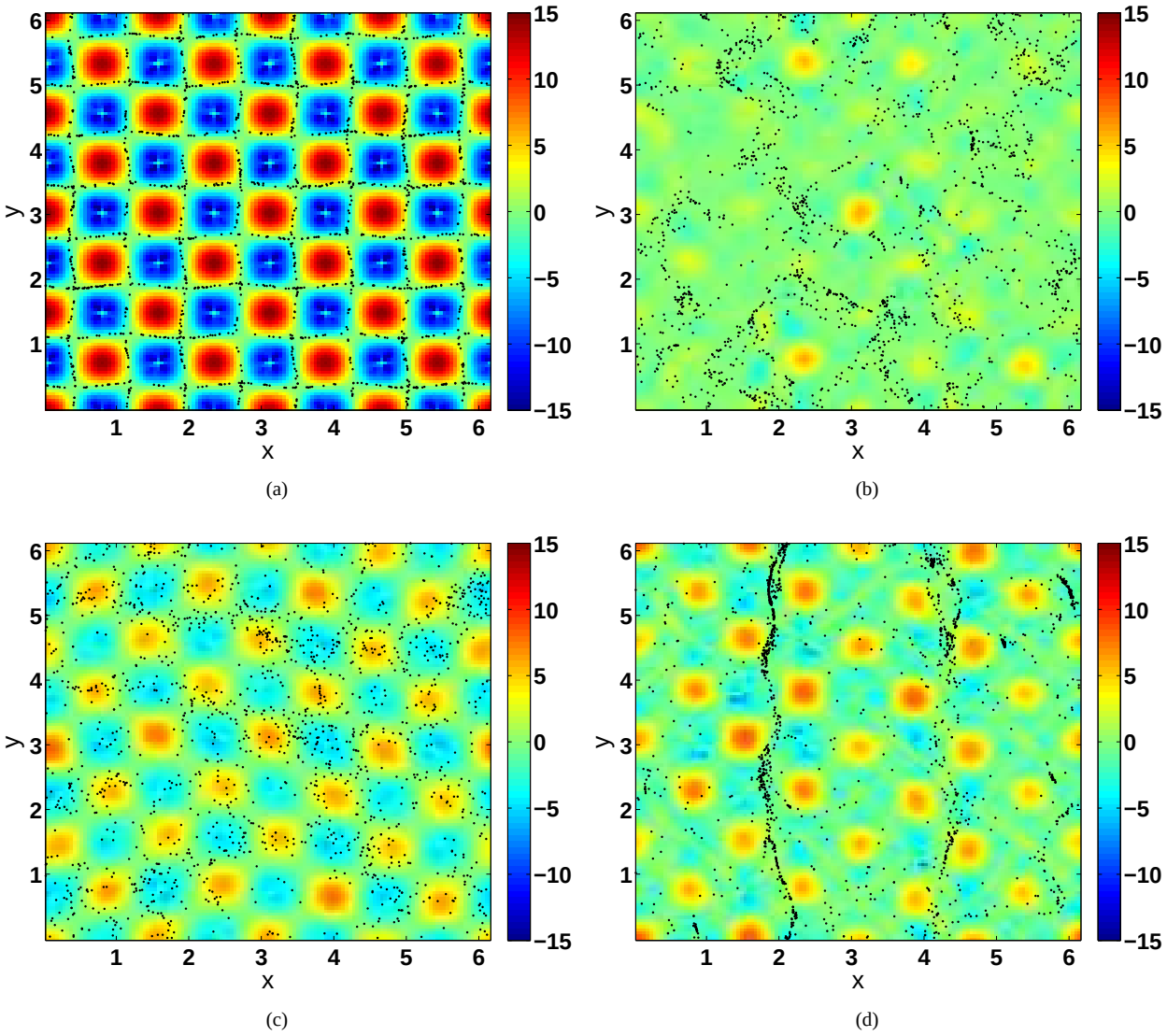

Figure 16. Particle positions (black dots) superimposed on pseudocolor plots of the Okubo-Weiss field Λ for (a) $\Omega = 1$ and $\tau_P = 1$ (crystalline phase), (b) $\Omega = 1$ and $\tau_P = 20$ (melted crystal in the elastic-turbulence regime), (c) $\Omega = 22$ and $\tau_P = 0.5$ (frozen crystal), and (d) $\Omega = 22$ and $\tau_P = 20$ (melted crystal in the dissipation-reduction regime).

14. Gupta, A., Perlekar, P. & Pandit, R. Two-dimensional homogeneous isotropic fluid turbulence with polymer additives. Phys. Rev. E **91**, 033013 (2015).

15. Groisman, A. & Steinberg, V. Elastic turbulence in a polymer solution flow. Nature **405**, 53–55 (2000).

16. Groisman, A. & Steinberg, V. Efficient mixing at low reynolds numbers using polymer additives. Nature **410**, 905–908 (2001).

17. Ganapathy, R. & Sood, A. Intermittency route to rheochaos in wormlike micelles with flow-concentration coupling. Physical review letters **96**, 108301 (2006).

18. Majumdar, S. & Sood, A. Universality and scaling behavior of injected power in elastic turbulence in wormlike micellar gel. Physical Review E **84**, 015302 (2011).

19. Braun, R., Feudel, F. & Seehafer, N. Bifurcations and chaos in an array of forced vortices. Physical Review E **55**, 6979 (1997).

20. Molenaar, D., Clercx, H., van Heijst, G. & Yin, Z. Attractor crisis and bursting in a fluid flow with two no-slip directions. Physical Review E **75**, 036309 (2007).

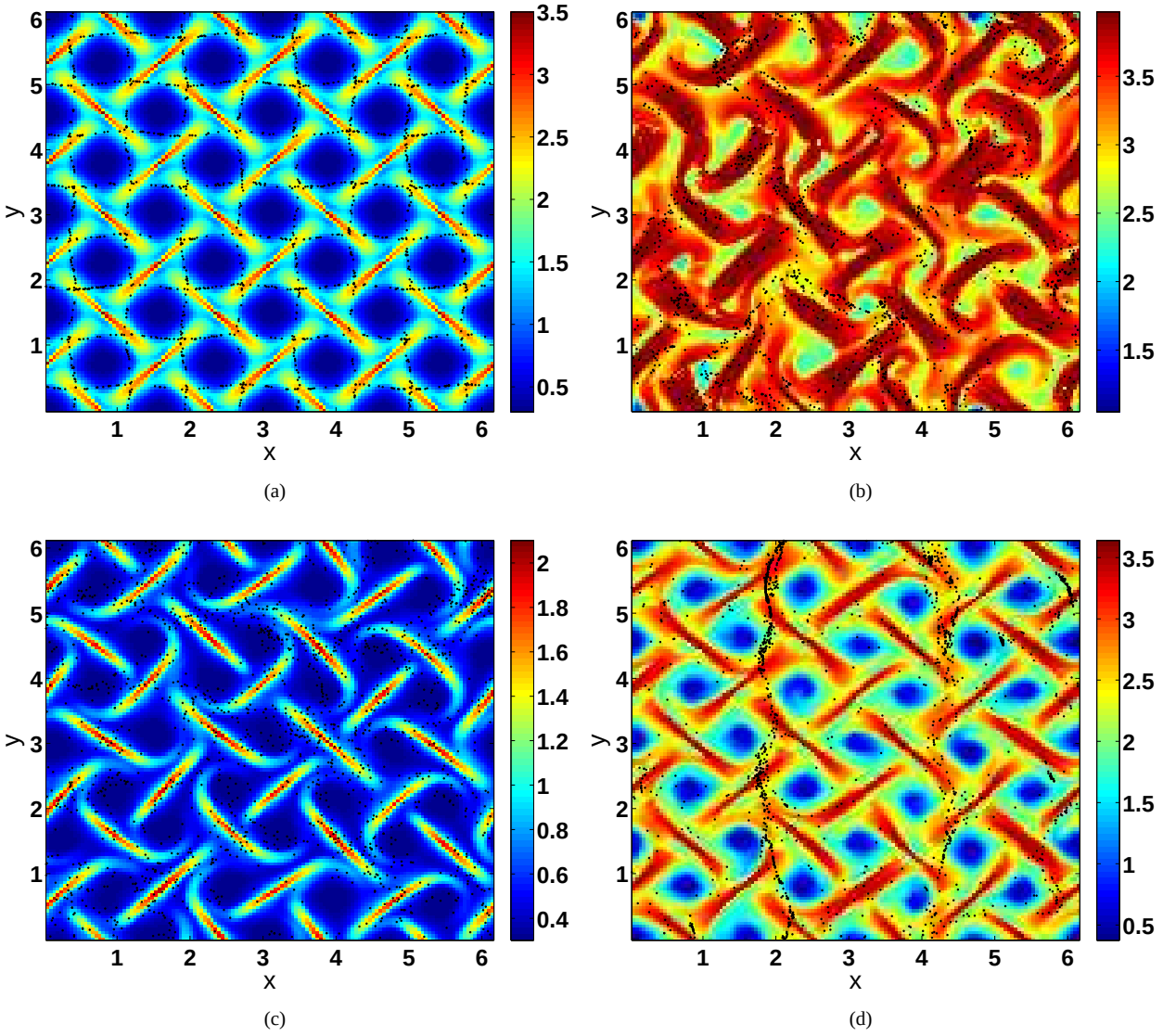

Figure 17. Particle positions (black dots) superimposed on a pseudocolor plot of the polymer stretching r_P^2 for (a) $\Omega = 1$ and $\tau_P = 1$ (crystalline phase), (b) $\Omega = 1$ and $\tau_P = 20$ (melted crystal in the elastic-turbulence regime), (c) $\Omega = 22$ and $\tau_P = 0.5$ (frozen crystal), and (d) $\Omega = 22$ and $\tau_P = 20$ (melted crystal in the dissipation-reduction regime).

21. Berti, S., Bistagnino, A., Boffetta, G., Celani, A. & Musacchio, S. Two-dimensional elastic turbulence. Physical Review E **77**, 055306 (2008).

22. Berti, S. & Boffetta, G. Elastic waves and transition to elastic turbulence in a two-dimensional viscoelastic kolmogorov flow. Physical Review E **82**, 036314 (2010).

23. Chomaz, J. & Cathalau, B. Soap films as two-dimensional classical fluids. Physical Review A **41**, 2243 (1990).

24. Chomaz, J. The dynamics of a viscous soap film with soluble surfactant. Journal of Fluid Mechanics **442**, 387–409 (2001).

25. Perlekar, P. & Pandit, R. Statistically steady turbulence in thin films: direct numerical simulations with ekman friction. New Journal of Physics **11**, 073003 (2009).

26. Okubo, A. Horizontal dispersion of floatable particles in the vicinity of velocity singularities such as convergences. In Deep Sea Research and Oceanographic Abstracts, vol. 17, 445–454 (Elsevier, 1970).

27. Weiss, J. The dynamics of enstrophy transfer in two-dimensional hydrodynamics. Physica D: Nonlinear Phenomena **48**, 273–294 (1991).

28. Rivera, M., Wu, X.-L. & Yeung, C. Universal distribution of centers and saddles in two-dimensional turbulence. Physical Review Letters **87**, 044501 (2001).

29. Elhmaïdi, D., Provenzale, A. & Babiano, A. Elementary topology of two-dimensional turbulence from a lagrangian viewpoint and single-particle dispersion. Journal of Fluid Mechanics **257**, 533–558 (1993).

30. Platt, N., Sirovich, L. & Fitzmaurice, N. An investigation of chaotic kolmogorov flows. Physics of Fluids A **3**, 681 (1991).

31. Vaithianathan, T. & Collins, L. R. Numerical approach to simulating turbulent flow of a viscoelastic polymer solution. Journal of Computational Physics **187**, 1–21 (2003).

32. Virk, P. S. Drag reduction fundamentals. AIChE Journal **21**, 625–656 (1975).

33. Kurganov, A. & Tadmor, E. New high-resolution central schemes for nonlinear conservation laws and convection–diffusion equations. Journal of Computational Physics **160**, 241–282 (2000).

34. Frigo, M. & Johnson, S. G. Fftw user's manual. Massachusetts Institute of Technology (1999).

35. Maxey, M. R. & Riley, J. J. Equation of motion for a small rigid sphere in a nonuniform flow. Physics of fluids **26**, 883 (1983).

36. Gatignol, R. The faxén formulae for a rigid particle in an unsteady non-uniform stokes flow. J. Mec. Theor. Appl **1**, 143–160 (1983).

37. Bec, J. et al. Acceleration statistics of heavy particles in turbulence. Journal of Fluid Mechanics **550**, 10 (2006).

38. Boffetta, G., De Lillo, F. & Gamba, A. Large scale inhomogeneity of inertial particles in turbulent flows. Physics of Fluids **16**, L20 (2004).

39. De Lillo, F., Boffetta, G. & Musacchio, S. Control of particle clustering in turbulence by polymer additives. Physical Review E **85**, 036308 (2012).

40. Schneider, T. M., Eckhardt, B. & Yorke, J. A. Turbulence transition and the edge of chaos in pipe flow. Physical review letters **99**, 034502 (2007).

41. Shajahan, T., Sinha, S. & Pandit, R. Spiral-wave dynamics depend sensitively on inhomogeneities in mathematical models of ventricular tissue. Physical Review E **75**, 011929 (2007).

42. Shajahan, T., Nayak, A. R. & Pandit, R. Spiral-wave turbulence and its control in the presence of inhomogeneities in four mathematical models of cardiac tissue. PloS one **4**, e4738 (2009).

43. Sahoo, G., Mitra, D. & Pandit, R. Dynamo onset as a first-order transition: Lessons from a shell model for magnetohydrodynamics. Physical Review E **81**, 036317 (2010).

44. Ray, S. S. & Vincenzi, D. Elastic turbulence in a shell model of polymer solution. arXiv preprint arXiv:1603.01692 (2016).

Author contributions statement

A.G. and R.P. conceived the simulations, A.G. conducted the simulations, A.G. and R.P. analysed the results. All authors wrote and reviewed the manuscript.

Additional information

The authors declare that they have no competing financial interests.